Composites Part B 287 (2024) 111786

Contents lists available at ScienceDirect

Composites Part B

journal homepage: www.elsevier.com/locate/compositesb

Impact characteristics of S2-glass fibre/FM94-epoxy composites under high and cryogenic temperatures: Experimental and numerical investigation

Ahmad S.M. Al-Azzawi [a,b], C.A. Featherston [b], Colin Lupton [c], Chulin Jiang [d], Antigoni Barouni [c], Ugur Koklu [e,f], Khaled Giasin [c,*]

[a] College of Engineering/Al-Mussaib, University of Babylon, Babylon, Iraq
[b] School of Engineering, Cardiff University, The Parade, Cardiff, CF24 3AA, UK
[c] School of Mechanical and Design Engineering, University of Portsmouth, Portsmouth, PO1 3DJ, UK
[d] Teesside University, Campus Heart, Southfield Rd, Middlesbrough TS1 3BX, UK
[e] Karamanoglu Mehmetbey University, Faculty of Engineering, Department of Mechanical Engineering, Turkey
[f] Department of Mechanical Engineering, Recep Tayyip Erdogan University, Rize, Türkiye

ARTICLE INFO

Handling Editor: Prof. Ole Thomsen

Keywords:
Low-velocity impact
Temperature effect
Glass-fibre composite
Damage mechanisms
Finite element analysis

ABSTRACT

The aerospace industry uses glass fibre reinforced polymer (GFRP) composites to manufacture structural and non-structural parts of an aircraft as they possess superior strength to weight ratio and exceptional corrosion resistance. Commercial aircraft operate in a very wide temperature ranges from −54 to 55 °C. Potential GFRP laminates are susceptible to impact during aircraft operation, and the temperature at impact governs the nature of damage and failure mechanisms. As a result, the current study focuses on examining how aeronautical GFRP composites behave in various temperature environments that are encountered during high- and low-altitude operations. Using S2-glass fibre/FM94-epoxy unidirectional prepreg, GFRP plates were created. Drop weight impact tests were conducted at ambient (25 °C), high (50, 75, 100 °C), and low (−25, −55 °C) temperatures, as well as at various impact energies (75, 150, 225 J). The damages were assessed visually, along with their sizes. Each testing scenario's impact parameters, including the impact load, deflection, and energy absorption, were also examined. In Abaqus/Explicit, a coupled temperature-displacement numerical model was created to predict the onset of stress and damage. According to experimental findings, GFRP plates are stiffer and show less apparent damage at cryogenic temperatures (~15–34 % lower displacement) than they do at other temperatures. Furthermore, it was observed that the matrix softens at high temperatures, showing larger damaged area at entry but with less obvious damage and increasing energy absorption, while semi-perforation occurred under cryogenic temperatures at entry with smaller damaged area. A strong correlation is shown between the experimental and FE data, confirming the capability of FE models to predict impact damage and deflections at different temperatures in the future.

1. Introduction

Due to their attractive thermo-mechanical properties, the aerospace industry utilises significant amounts of polymer-based composite materials such as CFRP and GFRP (Carbon or glass fibre reinforced plastics) in aircraft primary and secondary structures. It is common for a commercial aircraft to be exposed to temperature fluctuations during flight, take-off and landing. This mainly depends on several factors such the weather conditions and flying speed which sets design consideration for the structural performance of the materials used in the aircraft. For example, the maximum operating temperature at ground level during take-off and landing in commercial aircrafts ranges between −54 °C and +55 °C [1]. This can even become greater when operating at higher altitudes (i.e. up to 12000 m) where temperatures can be as low as −80 °C [2]. Past and future supersonic commercial aircraft skin's temperatures could be exposed to up to 120 °C when exceeding Mach 2 [3]. Damage mechanisms such as delamination, matrix cracks and fibre breakage are considered crucial failure modes in composite structures design investigations [4–7]. Resistance to these damage mechanisms is significantly affected by temperature and it is therefore necessary to ensure its effects are considered in predicting damage behaviour. When a composite structure is subjected to such impact scenarios, several

* Corresponding author.
E-mail address: khaled.giasin@port.ac.uk (K. Giasin).

https://doi.org/10.1016/j.compositesb.2024.111786
Received 6 March 2024; Received in revised form 31 July 2024; Accepted 20 August 2024
Available online 22 August 2024

damage mechanisms related to fibre and matrix failure can exist simultaneously [8,9]. Brittle and ductile damage characteristics of composite laminates must be investigated thoroughly when they are used in aeronautical structures at different environmental conditions (elevated and cryogenic temperatures), particularly when an impact event takes place [10]. Previous studies have shown that the fibre-reinforced composites with highly cross-linked matrices have limited resistance to impact loading [11–14], while delamination in thin laminates and fibre breakage in thicker laminates are the two main failure modes observed during impact and mainly caused by bending stresses [15]. Previous studies also showed that glass/epoxy composites with cross-ply laminates have better impact resistance than unidirectional laminates [16,17]. Depending on the temperature, the toughness and brittleness of FRP composite structures can vary, thus affecting their suitability, especially in impact events [10]. High and low temperatures affect the glass transition temperature (T_g) of the epoxy matrix and alters the mechanical properties of the composite and its energy absorption capacity, which, in turn, influences the failure mechanisms [18]. Glass transition temperature (T_g) for adhesive resin polymers is mostly considered a crucial design factor of composite laminates including polymers. Typical service temperatures for thermoset resin-based polymer composites are preferably below T_g but may be higher in aeronautical applications [19]. However, when reaching T_g, these materials will be subjected to a significant reduction in their stiffness.

Comprehensive research has been carried out to study how low temperature, interlayer reinforcement structure, and stacking sequence affect the mechanical properties of FRPs under low velocity impact (LVI) [20–24]. The behaviour of laminated GFRP composites across a temperature range of −60 °C–20 °C shows that even an impact energy of 20 J had a considerable impact on the variation of impact characteristics. As the temperature decreases, catastrophic fibre damage became more pronounced, and the perforation threshold increases [24]. However, other studies showed that the size of the damage and the deflection in GFRP laminates subjected to impact decreased with the decrease in temperature attributed to the ductile-to-brittle transition [25]. Polymers exhibit different mechanical characteristics at different temperatures leading to a decrease in modulus and strength with decreasing temperature [26]. The cryogenic temperatures increases the contractions in the epoxy which in turn enhanced interfacial fibre/matrix bonding and further tightening the fibres [25]. Khojin et al. [27,28] found that the maximum deflection increased with the increase of impact energy and temperature during LVI on Kevlar/glass fibre composite. Results also showed that the initial damage on the back side of the specimens and fibre breakage decreased significantly at high temperatures, while results for low temperatures revealed that the maximum impact damage occurs at −50 °C. The elastic modulus and tensile strength of a composite can reduce drastically by 55–94 % and 45–81 %, respectively, due to rise in temperature [29]. Additionally, it was previously observed that the absorbed energy increasingly depends on temperature as the energy level rises [27,28]. At low temperatures, laminates have a lower compressive strength compared with those tested at room temperature [30]. Icten et al. [24] found that the severity of perforation due to LVI of GFRP composites increased with the decrease in temperature from 60 to −20 °C. Li et al. [31] concluded that the FE model can be considered a good candidate for modelling impact damage under variant temperature conditions compared to the rule of the mixture and Chamis model at room temperature. T. Gómez del Río et al. [23] developed an FE model to study the effect of temperature on impact damage in CFRP tape laminates under LVI and found that matrix cracking and delamination are significantly affected by low temperature, while matrix crushing, and fibre failure occur in a small region regardless of the energy or temperature level. J. Weng et al. [52] investigated LVI characteristics and residual tensile/compressive strength of CFRP laminates at high temperatures both experimentally and analytically. A new integrated stress-based delamination failure criterion combined with extended Hashin failure criteria FE model has been established to simulate LVI damage and residual tensile and compressive strength of composite laminates at high temperatures. The impact damage and residual tensile/compressive strength were accurately predicted using the current model.

To the best of the authors' knowledge, very few studies have been presented considering impact damage characteristics of composite laminates at both high and very low temperatures coupling the effects of both thermal and mechanical stresses. In addition, the majority of the GFRP impact studies were on E-glass, carried out using thin laminates below 3.2 mm and low energies up to 70 J as evident in Appendix A, while this study included higher impact energy levels and higher laminates thickness. This research has included both experimental (meso-scale and microstructure laminates) and numerical investigations which enabled further understanding of damage characteristics of glass-fibre composite laminates at both high and low temperatures under LVI loading including the load carrying capacity, energy absorption, and damage modes. The three-dimensional multiscale numerical model implemented in this work, including thermal as well as mechanical strains, enables accurate predictions for in-service LVI at different temperatures, characterising and comparing the properties of glass-fibre composites at a range of LVI loads at these temperature extremes. The high-fidelity FE model included ply-by-ply model for composite laminate simulation considering the real thickness for each ply meshed separately and also including interlaminar cohesive layers between each two plies for delamination modelling is considered a great challenge in this work which helps in accurate prediction for composite laminate behaviour under impact loading with variant temperatures. It is focused on the unidirectional glass-fibre composites ''S2-glass fibre/FM94-epoxy'' used for aerospace applications but could also utilised for predicting impact damage behaviour in other composites subjected high and low temperatures during their application. The inclusion of thermal as well as mechanical strains, enables accurate predictions for in-service LVI at different temperatures, characterising and comparing the properties of glass-fibre composites at a range of LVI loads at these temperature extremes. Moreover, the brittle and ductile damage characteristics of composite laminates must be investigated thoroughly when they are used in aeronautical structures at different environmental conditions (elevated and cryogenic temperatures), particularly when an impact event takes place [10] which has been considered in this study.

2. Materials and methods

2.1. Specimen design and manufacturing process

For the impact tests, as indicated in Fig. 1a, prepregs containing unidirectional S2-glass fibres and FM94 epoxy resin were utilised to fabricate the panels. The panels are square with 240 mm length and 4.25 mm thick which were then cut into 70 mm square plates. A total of 32 prepregs were stacked in $[0°/90°/90°/0°]_{4s}$ similar to stacking used in aircraft structures [17,32]. As seen in Fig. 1b, the panels were cured in an autoclave set at 120 °C and 6 bars of pressure. An impactor with a 20 mm spherical diameter was used as seen in Fig. 1c [17] and using a CEAST 9350 impact machine. Table 1 shows the impact energy and temperature combinations used in the study. Each combination (i.e. of energy and temperature) was tested on three different specimens. Therefore, a total number of 45 impact tests were carried out. The results were also compared against impact tests conducted at room temperature (i.e. 25 °C) from a previous study [17]. The impact machine thermal chamber was heated/cooled to the designated temperature level. After that, the specimen was placed inside the thermal chamber and kept there for ~45 min to reach thermal equilibrium with the set temperature of the thermal chamber. After that, the impact test was carried out at the designated energy level.

Every test carried out in this research has an initial velocity of approximately 4.44 m/s, making them all low-velocity impact tests. The force versus displacement and energy versus time data presented are all

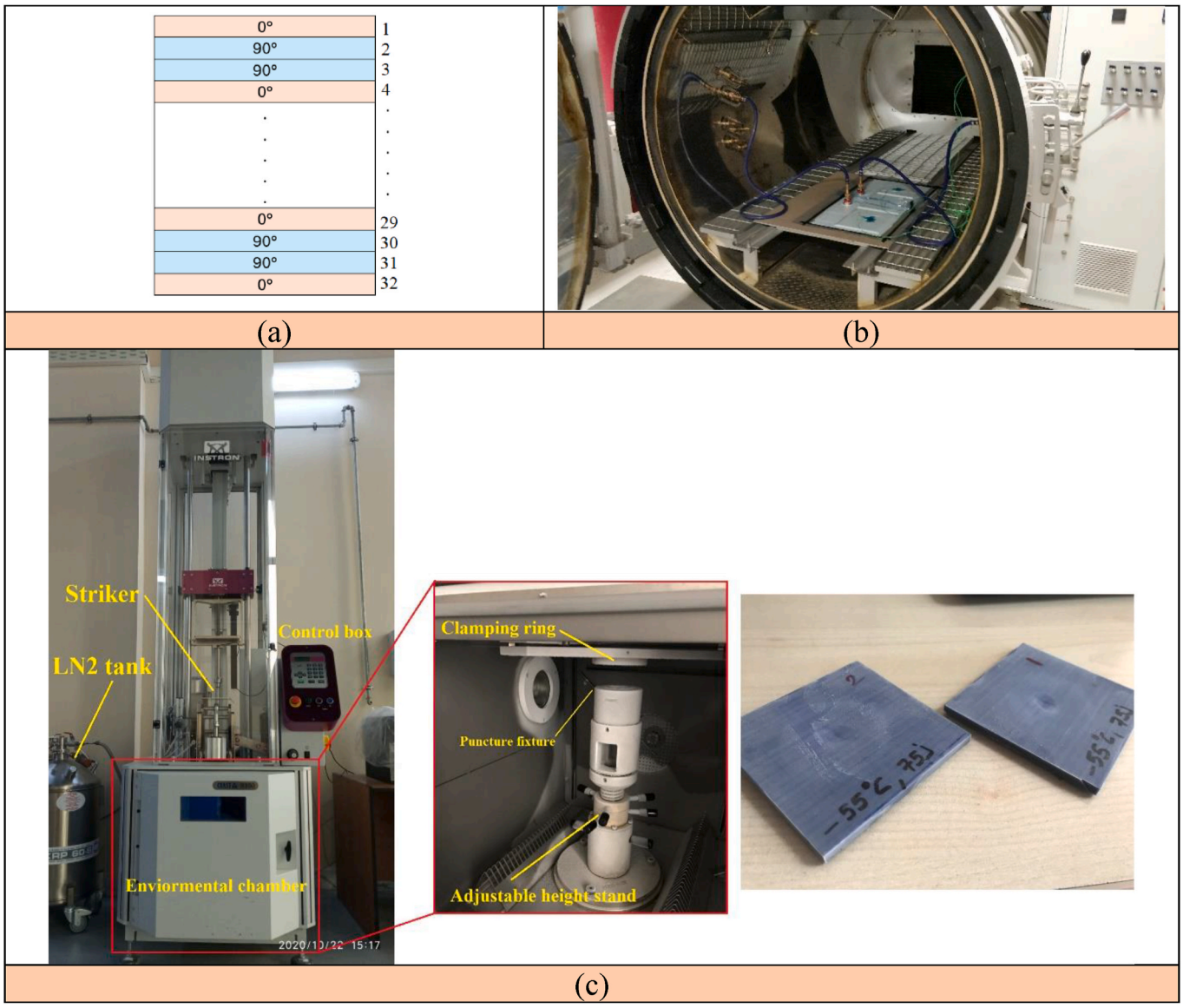

Fig. 1. Fabrication of test specimens showing (a) Layup configuration (b) Curing setup in autoclave [17,33] (c) impact test machine and post-impact specimens.

Table 1
Energy and temperature levels.

Test No.	Energy (J)	Temperature (°C)
1	75	−50
2	75	−25
3	75	50
4	75	75
5	75	100
6	150	−50
7	150	−25
8	150	50
9	150	75
10	150	100
11	225	−50
12	225	−25
13	225	50
14	225	75
15	225	100

the mean values of these three repetitions, resulting in a total of 15 impacted samples for each energy level. The study's impact energy levels were chosen based on previously published research on the effects of glass fibre composites and fibre orientation [17]. Using a Nikon XT H 225 X-ray micro-CT (computed tomography) scanner, the plates were scanned following the impact tests in order to evaluate internal damage and failure mechanisms. The extent of damage in each panel determined the range of resolutions that were used, which was approximately 47 μm–162 μm. The scanned data was processed and analysed using MyVGL 3.5.2 software. To examine the failure phenomena and damage mechanisms in the samples in more detail, scanning electron microscopy was employed. One sample was cross sectioned from the centre of each energy/temperature level for this purpose. The sliced samples were then sputter-coated and examined under two SEM microscopes at various magnifications and wide field view.

3. Finite element model

A three-dimensional finite element model of the composite laminate was generated in Abaqus software. A ply-by-ply high fidelity technique was used considering 0.133 mm thickness for each ply [29] in order to achieve the real total thickness of the specimen 4.25 mm for 32 plies of fibre composite, and with setting a specific orientation for each layer with either (0°) or (90°) in order to simulate stacking sequence discussed

earlier in Section 2.1. The cohesive layers were meshed using the layer-by-layer technique and were then connected to the neighbouring composite plies using the tie constraint method which couples all nodes in the three-coordinate axes. A high-accuracy structured mesh was created in order to simulate all constituent layers for the laminate as shown in Fig. 2. The constituent composite layers were meshed using continuum shell elements (SC8R), while for interlaminar cohesive layers, a three-dimensional cohesive element (COH3D8) has been used. The later elements included a thickness of 0.01 mm and a mesh size length of 1 mm (thickness for the cohesive elements was identified based on a previous FE analysis on similar fibre laminate structures and the mesh size was considered based on mesh sensitivity investigations) [34–37]. The impactor was meshed using a discrete rigid element (R3D4) since its deformation was negligible during the impact analysis. The inertia mass of the impactor was estimated based on the kinetic energy level used in the experiments.

Prescribed temperatures were applied to the laminate using pre-defined field (temperature type) boundary conditions for initial and propagated temperatures. This ensured the required temperature was applied before applying the impact load, allowing for the introduction of stresses due to differential thermal expansion using the coefficients given in Table 2 and coupling these thermal stresses with the mechanical stresses generated by the impact loads. The Hashin damage theory was used for modelling damage in the composite layers (as detailed in section 3.1), with the constituent composite material properties given in Table 2. Built-in boundary conditions have been used to simulate fixed edges of the clamps in the tests as shown previously in Fig. 2. Pre-defined temperature initial conditions were introduced to the model in order to simulate the thermal stresses produced from temperatures applied in the experiments, based on the thermal expansion coefficients given in Table 2.

Following this, the specimens were subjected to low-velocity impact loads which are introduced using velocity control boundary condition loading through the impactor. The cohesive zone model method (CZM) was used to model damage in the interlaminar cohesive layers (as detailed in section 3.2). The interfacial material properties required to completely define the CZMs used in this work are provided in Table 3.

Table 2
S2-glass fibre/FM94-epoxy resin composite material properties [38–40].

Parameter	Value
Young's modulus (MPa)	
E_{11}	50000
E_{22}	9000
Poisson's ratio	
ν_{12}	0.33
ν_{23}	0.04
Shear modulus (MPa)	
G_{12}	3500
G_{23}	3000
Tensile strength (MPa)	
X_T	2000
X_C	550
Y_T	43
Y_C	90
Shear strength (MPa)	
S_{12}	93
S_{23}	50
Critical Strain Energy Release Rate (SERR) (kJ/m^2)	
$G_{C,X}$	12.0
$G_{C,Y}$	1.0
Density, ρ [39] (kg/m^3)	2000
Coefficient of thermal expansion (1/°C)	
α_{11} [40]	6.1×10^{-6}
α_{22} [40]	26.2×10^{-6}

3.1. Hashin damage criterion

The Hashin damage theory [42] has been utilised for predicting damage behaviour in composite laminates. This criterion included both fibre and matrix failure modes and more details about this theory are given in Ref. [41]. The Hashin damage initiation Equation for fibre tension (d_{ft}) is as follows:

$$\left(\frac{\sigma_{11}}{X_T}\right)^2 + \left(\frac{\sigma_{12}}{S_{12}}\right)^2 = 1 \quad (1)$$

while damage initiation according to the Hashin theory under fibre compression (d_{fc}) is,

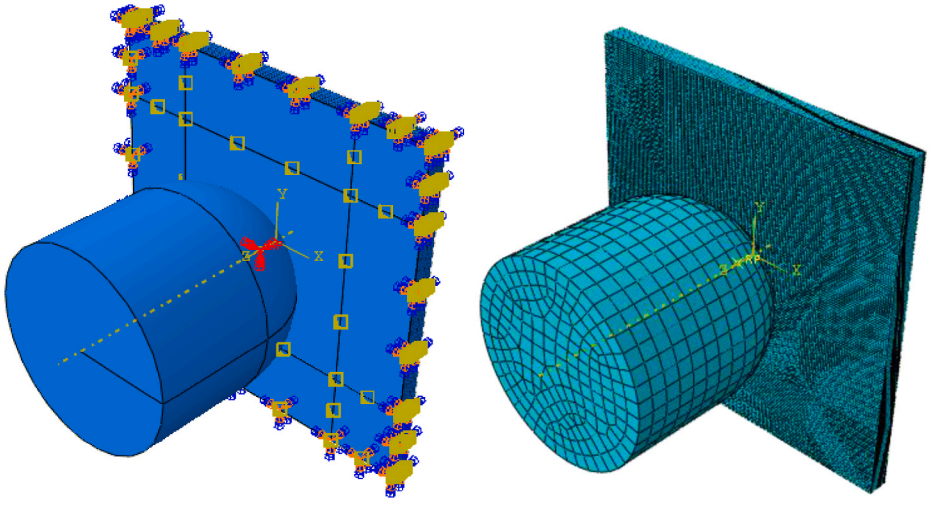

Fig. 2. FE model of the composite plate and the impactor including mesh design (left), boundary conditions and applied loads (right).

Table 3
Cohesive properties including adhesive epoxy resin FM94 [41].

t_n^0 (MPa)	t_s^0 (MPa)	t_t^0 (MPa)	G_n (kJ/m^2)	G_s (kJ/m^2)	G_t (kJ/m^2)	E/E_{nn} (GPa/mm)	$G1/E_{ss}$ (GPa/mm)	$G2/E_{tt}$ (GPa/mm)
50	50	60	4.0	4.0	4.0	10^5	10^5	10^5

$$\left(\frac{\sigma_{11}}{X_C}\right)^2 = 1 \tag{2}$$

X_T and X_C are the ultimate tensile and compressive strength, respectively, and S_{12} is the in-plane shear strength, σ_{11} and σ_{22} are the principal stresses in the fibre and transverse directions, respectively, and finally σ_{12} represent the in-plane shear stress. The Hashin damage initiation criterion for matrix tension (d_{mt}) is,

$$\left(\frac{\sigma_{22}}{Y_T}\right)^2 + \left(\frac{\sigma_{12}}{S_{12}}\right)^2 = 1 \tag{3}$$

while the criterion for matrix compression (d_{mc})damage initiation is,

$$\left(\frac{\sigma_{22}}{2\,S_{12}}\right)^2 + \left[\left(\frac{Y_C}{2\,S_{12}}\right)^2 - 1\right]\frac{\sigma_{22}}{Y_C} + \left(\frac{\sigma_{12}}{S_{12}}\right)^2 = 1 \tag{4}$$

where Y_T and Y_C are the tension and compression strengths in the transverse-direction, respectively.

Damage evolution in composite plies can be calculated using the following formula: this cannot be achieved until the above damage initiation criterion is reached. Abaqus/Explicit analysis including converting strains into displacement using the characteristic length of each element in the FE model [43]. Then based on these damage variables we can calculate the two-dimensional stiffness matrix of damage C_d at each integration point as follows,

$$C_d = \frac{1}{D}\begin{bmatrix} (1-d_f)E_1 & (1-d_f)(1-d_m)\nu_{21}E_1 & 0 \\ (1-d_f)(1-d_m)\nu_{12}E_2 & (1-d_m)E_2 & 0 \\ 0 & 0 & (1-d_s)GD \end{bmatrix} \tag{5}$$

The total damage D can be calculated using the following criterion,

$$D = 1 - (1-d_f)(1-d_m)(\nu_{21}.\nu_{12})$$

Finally, the two-dimensional stress matrix σ can be calculated based on the two-dimensional strain matrix ε and the stiffness matrix of damage from Equation (5) [41] as follows,

$$\sigma = C_d.\,\varepsilon \tag{6}$$

The variable $\boldsymbol{d_f}$ represents fibre damage and $\boldsymbol{d_m}$ is the matrix damage while the variables $\boldsymbol{d_{ft}}$ and $\boldsymbol{d_{fc}}$ are the damage in fibre under tension and compression loads, respectively, also $\boldsymbol{d_{mt}}$ and $\boldsymbol{d_{mc}}$ are matrix damage under tension and compression loads, respectively. Also it's worth mentioning that $\boldsymbol{d_f}$ can be calculated from the variables $\boldsymbol{d_{ft}}$ and $\boldsymbol{d_{fc}}$ given in Equations (1) and (2), While $\boldsymbol{d_m}$ can be calculated from the variables $\boldsymbol{d_{mt}}$ and $\boldsymbol{d_{mc}}$ given in Equations 3 and 4. Where $\boldsymbol{d_f} = \left\{\begin{matrix} \boldsymbol{d_{ft}} \text{ if } \boldsymbol{\sigma_{11}} \geq \boldsymbol{0} \\ \boldsymbol{d_{fc}} \text{ if } \boldsymbol{\sigma_{11}} < \boldsymbol{0} \end{matrix}\right\}$ and $\boldsymbol{d_m} = \left\{\begin{matrix} \boldsymbol{d_{mt}} \text{ if } \boldsymbol{\sigma_{22}} \geq \boldsymbol{0} \\ \boldsymbol{d_{mc}} \text{ if } \boldsymbol{\sigma_{22}} < \boldsymbol{0} \end{matrix}\right\}$.

3.2. Cohesive zone model

A bilinear cohesive zone model (CZM) considering mixed-mode damage is developed to simulate delamination onset and evolution in the interlaminar layers of composite laminates. A quadratic nominal stress formula [41] has been used to obtain damage initiation in cohesive layers as follows,

$$\left(\frac{\langle\sigma_I\rangle}{\sigma_I^{max}}\right)^2 + \left(\frac{\sigma_{II}}{\sigma_{II}^{max}}\right)^2 = 1 \tag{7}$$

where $\langle - \rangle$ is the Macaulay bracket which refers to that the pure nominal compressive stresses do not develop damage initiation. The damage evolution in cohesive layers was modelled using the power law damage criterion [41] which includes the strain energy release rates G_I and G_{II} and the critical strain energies G_{Ic} and G_{IIc} for modes I and II respectively,

$$\left(\frac{G_I}{G_{Ic}}\right)^n + \left(\frac{G_{II}}{G_{IIc}}\right)^n = 1 \tag{8}$$

where n is a power law criterion coefficient and depends on the failure mode interaction (normal and shear) and its value can be assumed as a unity for the linear mix mode [44].

4. Results and discussion

The post-impact front and rear views of one batch of tested samples are shown in Fig. 3 and the sectioned micro-CT graphs are given in Fig. 4. The optical images and CT-graphs show the severity and various forms of damage that occurred due to impact using different energy levels and various temperatures. These images will be used to support the analysis and discussion in the following subsections. Several forms of damage occurred due to impact, mainly delamination and debonding, matrix cracking, fibre/matrix bulging due to incomplete penetration (semi-perforation) and strain crystallisation. A local indentation was formed at the centre of the front face of all the specimens due to the spherical impactor. The shape and size of the indentation and surrounding damage varies according to the energy and temperature levels used. The cracks on the front face of the specimens appear to propagate from the centre of the impact zone in four perpendicular directions as it can be seen from all the images in Fig. 3. The impact caused bending of the specimens which varied significantly depending on the energy and temperature levels which in return affected their failure characteristics. For example, in Fig. 3 (first row) which present images of the front of specimens tested at temperatures (50–100 °C) shows that they exhibited impact damage starting with partial fibre breakage in the 0° and 90° fibre plies indicated by the white lines (crazing) extending in the longitudinal and transverse directions of the specimens' surface, aligned with the fibre orientations. This is due to the lower shear strength and impact damage resistance of specimens at high temperatures leading to increased softening of the matrix. As the resin becomes weaker resulting in only the fibre layers carrying the applied loads leading to partial fibre damage in the 0°, 90° directions. Fig. 3 (first row) also shows that at 50–100 °C, the impact area at the front is circular and resembles the imprint caused by the spherical impactor. The impact area appears to increase with the rise in impact energy. Furthermore, at these higher temperatures, strain crystallisation is also noted on the front surfaces as seen by the white segments forming between the white lines, which appears to increase with temperature and energy level due to increased softening of the matrix. In addition, according to Figs. 3 and 4, the bending forces due to impact resulted in Fig. 3 (second row) shows that for higher temperatures, dome-like bulge is formed without penetration or fibre/matrix rupture. The size and height of the bulge appear to decrease with the rise of temperature which could be due to increased retention in fibre/matrix plies after impact. Images of the rear of the specimens also confirm that delamination and matrix cracks developed in the background GFRP layers and increased with the increment of applied impact energy. The front of the specimen is subjected to compression loading due to the bending forces caused by the impact which increases the delamination in the inner plies as it can be seen in

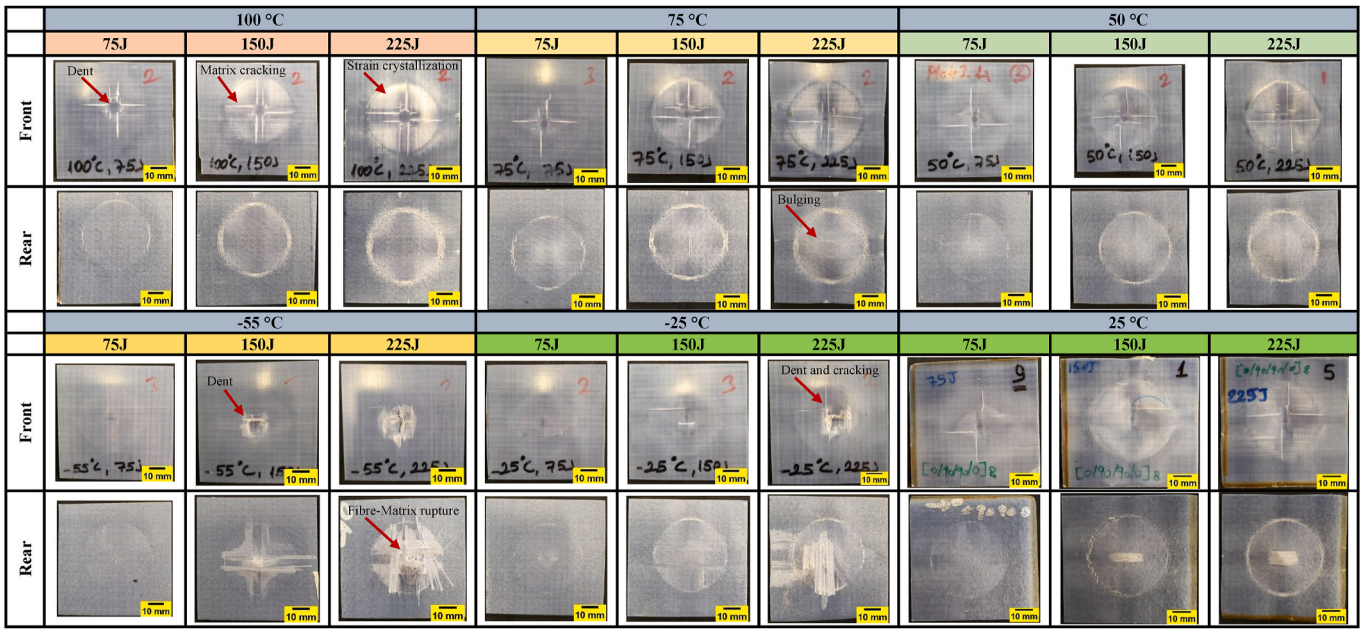

Fig. 3. Front and rear images of the experimental impact damage for the S2- glass fibre/FM94-epoxy specimens under impact energies 75 J,150 J and 225 J and temperature range between −55, and 25, 25 [17], 50, 75 and 100 °C.

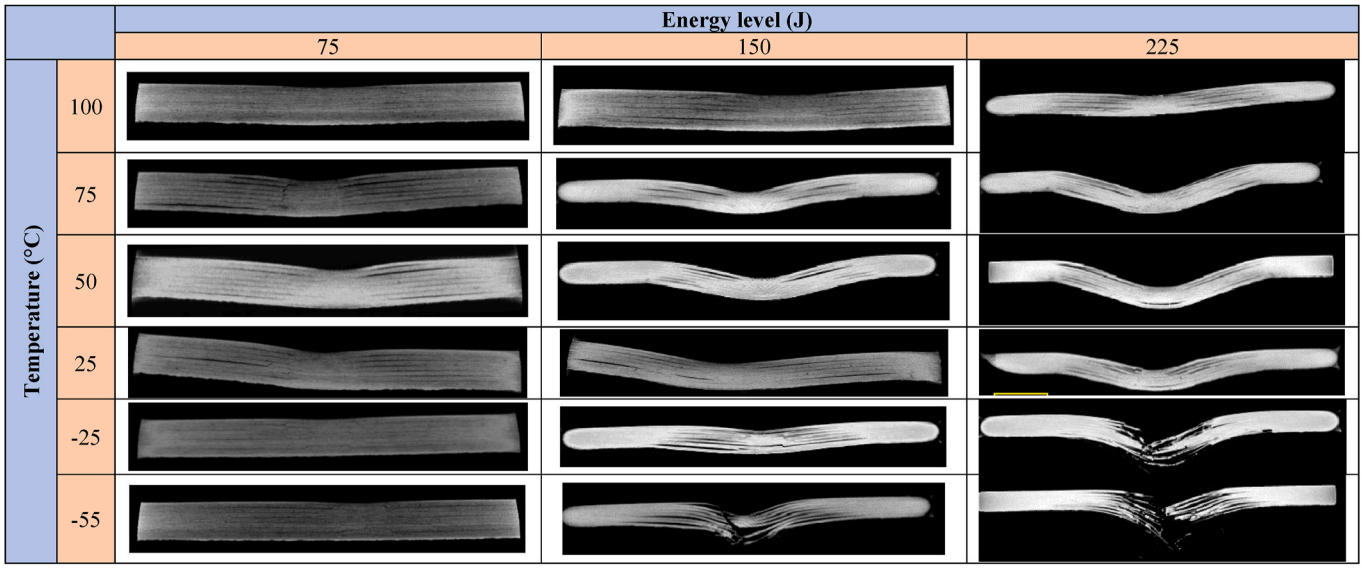

Fig. 4. Through-thickness C-scan images of the impact damage for the S2/FM94 glass fibre plates under impact energies 75 J,150 J and 225 J and temperature range between −55, and 25, 25 [17], 50, 75 and 100 °C.

specimens under temperatures of 25–100 °C.

Fig. 3 (third row) shows that at cryogenic temperatures (−25 and −55 °C) delamination was not observed, with only matrix cracks and shear damage in the middle of GFRP plates which increases with the increment of applied impact energy. This damage is mostly due to penetration in the centre of the plates particularly at higher impact energy levels. The main reason for such penetration is that the resin layers become more brittle at cryogenic temperatures as mentioned earlier which reduces their impact resistance. Fig. 3 (fourth row) presents that for room and cryogenic temperatures, at lower energy dome-like bulge is also noticed without penetration or fibre/matrix rupture. While at higher impact energy levels fibre/matrix damage is observed with partial penetration at lower temperatures as the resin layers become more brittle at cryogenic temperatures possibly due to a visco-elastic deformation behaviour. In addition, it can be said that the load deflection response in fibre/epoxy composites is rather a complex phenomenon which involves nonlinear material response as well as the varying contact area between the impactor and the plate that ultimately influences the contact friction behaviour and affect not only the strain rate/stresses but also the deflection behaviour of the plate [45]. Fig. 4 shows that matrix cracking and delamination are present under all impact energy levels and temperatures. The severity however varies significantly with minimal damage seen in samples impacted at 100 °C and 75 J. Maximum damage occurred at 150–225 J at cryogenic temperatures.

4.1. *Effect of low-impact energy level of 75 J*

Loads, displacements and kinetic energies were recorded for S2/FM94 glass fibre plates under 75 J impact energy at temperatures

between −55 and 100 °C as shown in Fig. 5, which presents both numerical and experimental results. From the experiments at room temperature and cryogenic temperatures between (−25 to −55 °C) tests present similar behaviour with the load increasing with time up to a maximum strength of about 25 kN. After that, the load drops sharply due mostly to fibre breakage as shown in Fig. 5a. Results for higher temperatures between (50–100 °C) exhibited a drop in compression strength with increasing temperature as resin layers reach their glass transition temperature (T_g) which leads to a reduction in their strength [46,47]. Similar behaviour was observed for all specimens tested at higher temperatures compared to those tested at lower temperatures (see Fig. 5). Load drops were also noticed for all specimens early on in the tests at about (1 *ms*). These were due to matrix cracking and matrix compression damage when the impactor first hit the specimens. The displacement curves in Fig. 5c show increasing displacement with increasing load for all specimens tested until the ultimate compressive strength is reached. At room temperature and cryogenic temperatures between (−25 to −55 °C), deformation reaches a maximum of 6 mm again mostly due to fibre and matrix compression damage. After this, displacements start to reduce due to the bridging of fibres in the cross-ply laminates which provide high resistance under impact loading reaching about half their maximum value at the end of the test [48]. As no penetration was occurred, thus impactor bounces back after hitting the specimen and this was noticed through reduction in the out-of-plane displacement which is reduced gradually up to the end of test. At higher temperatures (50–100 °C) out-of-plane deformation reaches up to 7–8.5 mm before reducing again to approximately half of their maximum value at the end of the test. For all specimens tested kinetic energy

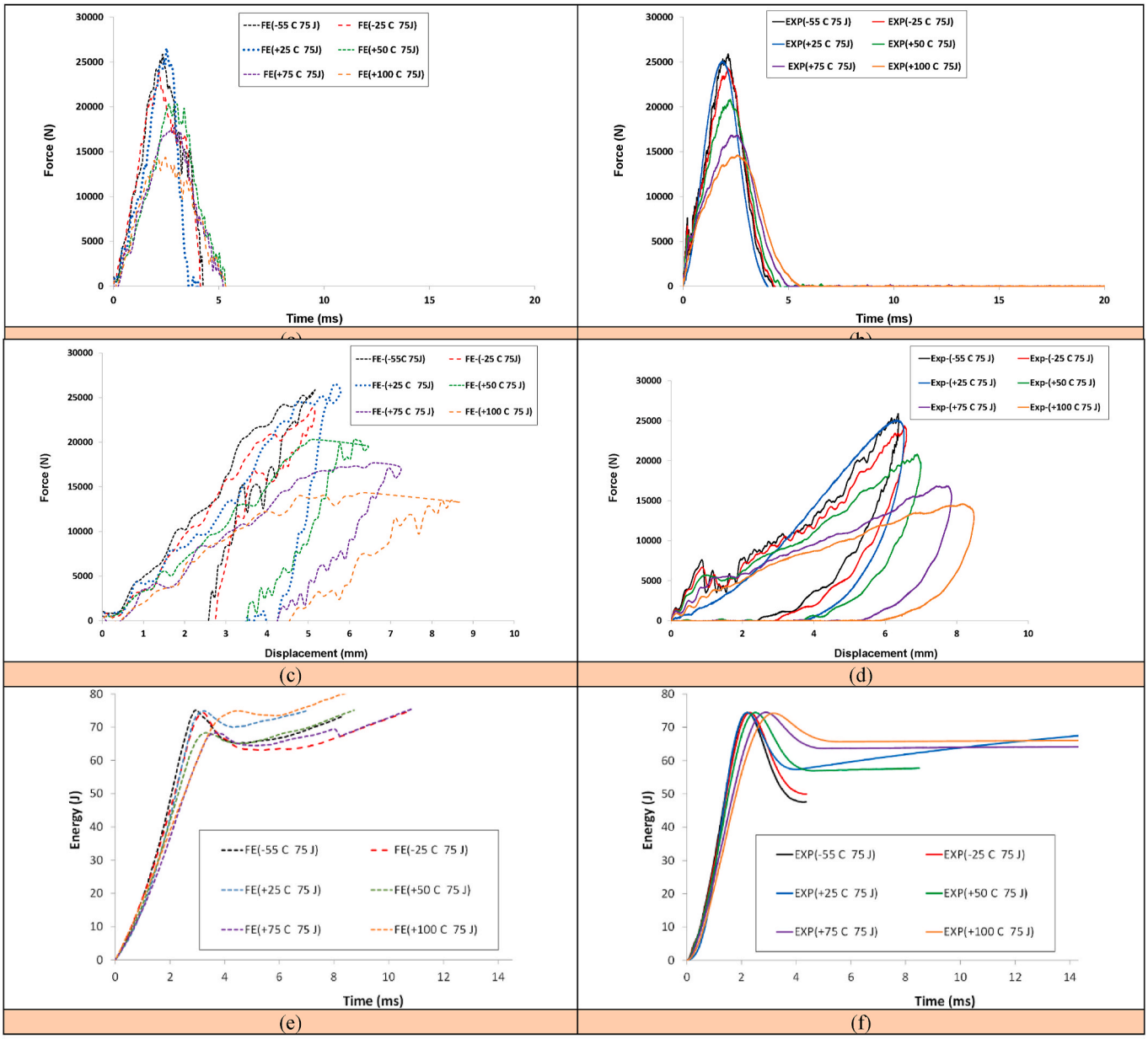

Fig. 5. Load vs. time; out-of-plane displacement curves and energy vs. time relation for S2- glass fibre/FM94 epoxy composite plates under 75 J impact energy at a temperature range −55, −25, 25 [17], 50, 75 and 100 °C, FE and experimental results.

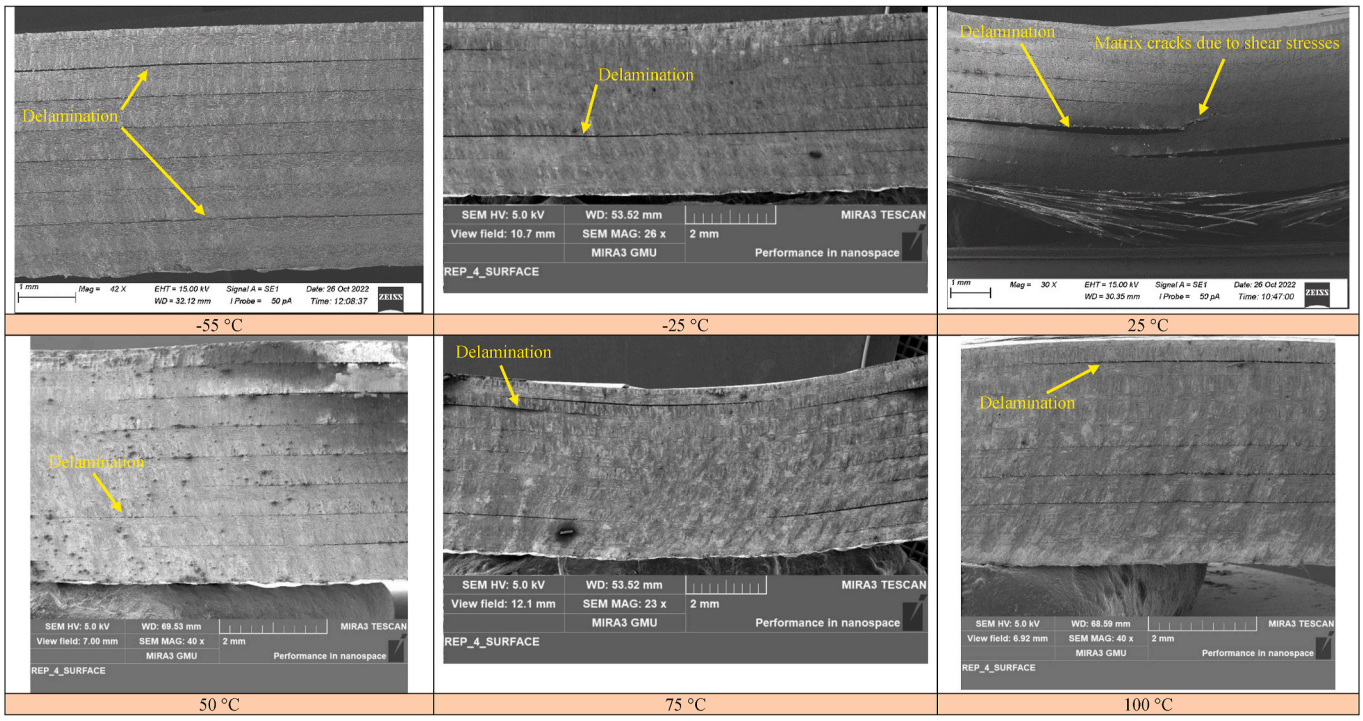

Fig. 6. SEM images for samples after impact at 75 J and different temperatures.

reaches a maximum value of 75 J as planned before reducing sharply for low and room temperature tests as shown in Fig. 5c. In contrast, for specimens tested at higher temperatures, energy reduced more gradually and then started to recover at a time (5 ms) remaining constant up to the end of the test.

Fig. 5 also presents the FE results, with excellent agreement between these and the experimental results in terms of maximum impact strength for all specimens over a range of temperatures. This exhibits the capability of the Abaqus/Explicit solver and the predefined thermal boundary conditions to simulate the coupling of thermal and mechanical impact under LVI. At the relatively low energy level of 75 J, FE results reveal significant effects due to thermal stresses in addition to mechanical stresses where specimens with cryogenic temperatures failed with a higher strength (23–25 kN) compared with those at higher temperatures (50–100 °C) which failed at 14–20 kN mostly due to the resin layers reaching their glass transition temperature. Comparison of the out-of-plane displacements between FE and experimental results also shows a good correlation up to the maximum impact strength although the FE results overestimate the displacement at the end of the test. This is thought to be a result of misalignments in extracting the displacement from the crosshead of the impact machine during the test and more advanced instrumentation (High-speed digital image correlation system) is recommended for future work. Finally observed energies are also successfully predicted as the FE model considers the effect of thermal stresses and mechanical impact stresses simultaneously. As can be seen from Fig. 6, the main damage in specimens under 75 J was delamination and matrix cracking which further confirms the previous discussion. Impact damage was more prevalent at temperature range of −25 to 75 °C where severe bending, delamination and fibre/matrix failure can be observed.

4.2. *Effect of medium impact energy level of 150 J*

The experimental results for specimens subject to 150 J impact energy at temperatures ranging between −55 and 100 °C are presented in Fig. 7. At room temperature and cryogenic temperatures between −25 and −55 °C tests present similar behaviour with load increasing to a maximum strength of about 30 kN, 5 kN higher than for an impact of 75 J as can also be seen in Section 4.1 Fig. 5. Again, following this point, there is a sharp drop in load but in this case, it was accompanied by a greater level of matrix cracking and compression due to the higher impact energy followed by fibre breakage as seen in Fig. 7a.

For higher temperatures (50–100 °C) the compression strength was reduced due to the resin layers reaching their glass transition temperature (T_g) reducing their strength [46,47]. A sharp drop was again noticed for all specimens at the beginning of the test due to matrix cracking and compression damage when the impactor first hits the specimens. Out-of-plane displacements for all specimens again increased with increasing load until the ultimate compressive strength. At room temperature and cryogenic temperatures between −25 and −55 °C deformation reached about 7–9 mm at maximum compression strength and then reduced reaching about half its maximum value at the end of the test. At higher temperatures (50–100 °C) out-of-plane deformation was higher, reaching 10–12 mm at maximum compression strength before falling to approximately half the maximum value at the end of the test as seen in Fig. 7b. Again, similar to previous results of 75 J energy, as no penetration occurred, thus impactor bounces back after hitting the specimen and this was noticed through reduction in the out-of-plane displacement which is reduced gradually up to the end of test. Finally, the kinetic energy after reaching a maximum value of 150 J reduced sharply for low and room temperatures but more gradually for higher temperatures as seen in Fig. 7c. Fig. 7 also presents an excellent correlation between FE results and experiments in terms of maximum impact strength for all specimens at different temperatures again showing the effect of the induced thermal stresses at higher temperatures with specimens at cryogenic temperatures failing with a slightly higher strength of about (33–35 kN) compared to those at room and higher temperatures (25–75 °C) which failed at (25–30 kN) reducing down to about 22.5 kN at 100 °C. A good correlation is also seen for impact displacements between FE results and experiments. Finally, observed energies were also accurately predicted through microstructure analysis represented by the SEM images, as seen in Fig. 8. In addition, SEM images reveals that the failure mechanism vary with temperature. The main damage forms at 150 J were delamination, matrix cracking and

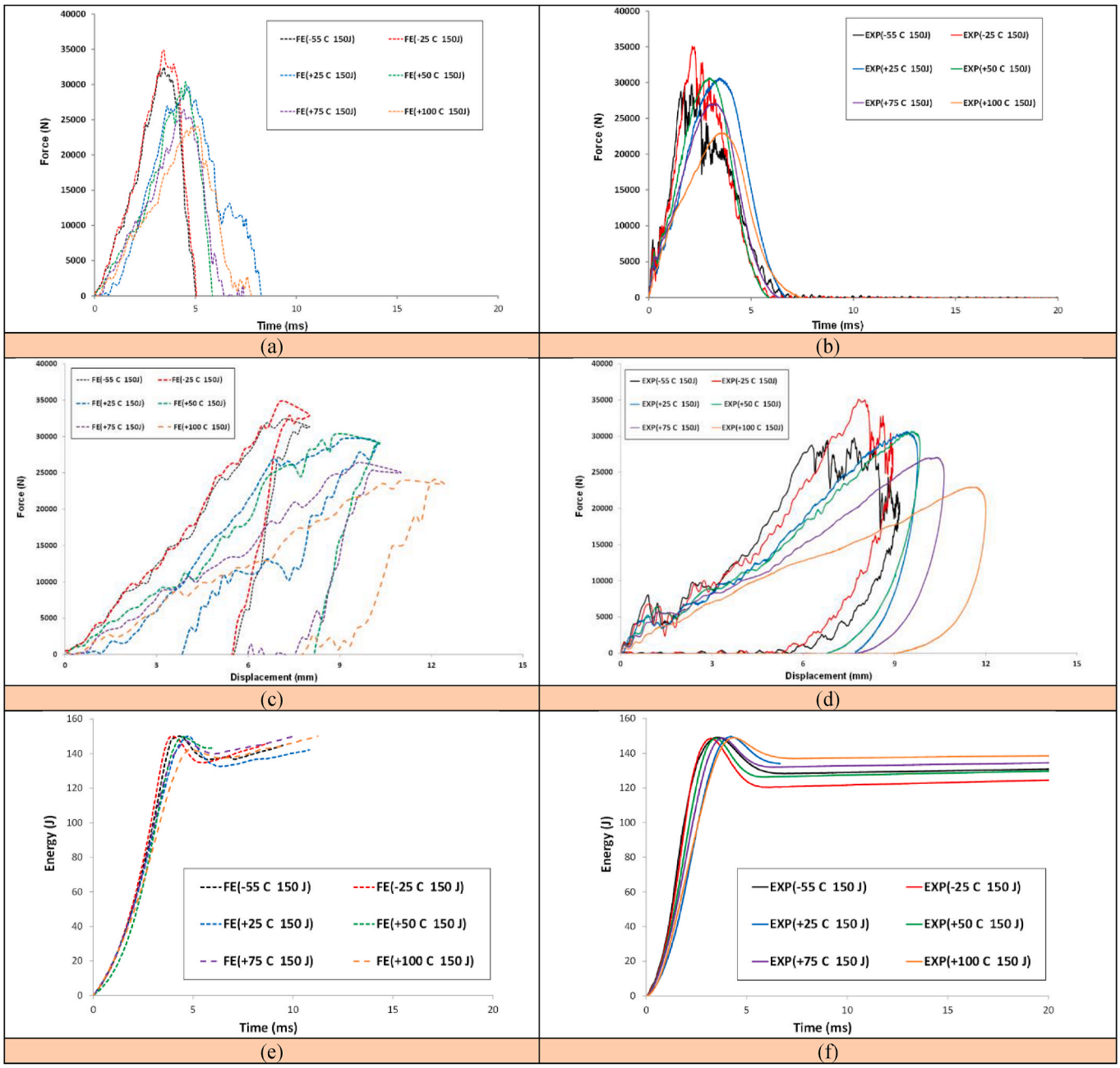

Fig. 7. Load vs. time; displacement curves and energy vs. time relation for S2/FM94 glass fibre plates under 150 J impact energy at a temperature range between −55, and 25, 25 [17], 50, 75 and 100 °C, FE and experimental results.

fibre/matrix rupture. Matrix cracking due to shear stresses mainly occurred at cryogenic temperatures (−25 and −55 °C) which is a clear indication of a brittle fracture/failure. This can be explained as follows: since the matrix is responsible for supporting the fibres when subjected to compressive loading [46], its increased stiffness at cryogenic temperatures shifts the failure from delamination due to bending stresses to matrix cracking failure due to shear stresses as shown in (−25 and −55 °C) Specimens in Fig. 8. The reduced matrix ductility at cryogenic temperatures limits it from yielding and therefore increases the damage in the laminate due to impact. Moreover, glass fibres contract in the axial traverse directions when cooled down which in return affects the stress-strain state of the fibre/matrix interface. Compressive stresses occur on the fibre/matrix interface since the matrix contraction is larger than that of the glass fibres [46], which could also explain the reduced damage tolerance of the specimens at cryogenic temperatures. Meanwhile, delamination appears to be the main failure mechanism in specimens impacted at 25–100 °C with complete absence of other failure modes. The difference in damage and failure mechanisms could be also attributed to the change in the molecular movement of the epoxy matrix with temperature (increased ductility) which in return affect the stress relaxation of the laminate and leads to higher damage tolerance due to impact. However, this is highly dependent on the molecular structure of the epoxy matrix.

4.3. *Effect of the high impact energy level of 225 J*

Loads, displacements and kinetic energies were recorded for S2/FM94 glass fibre specimens tested under impact energy of 225 J at a temperature range between (−55 and 100 °C) which are presented in Fig. 9, which shows the experimental results. At cryogenic temperatures

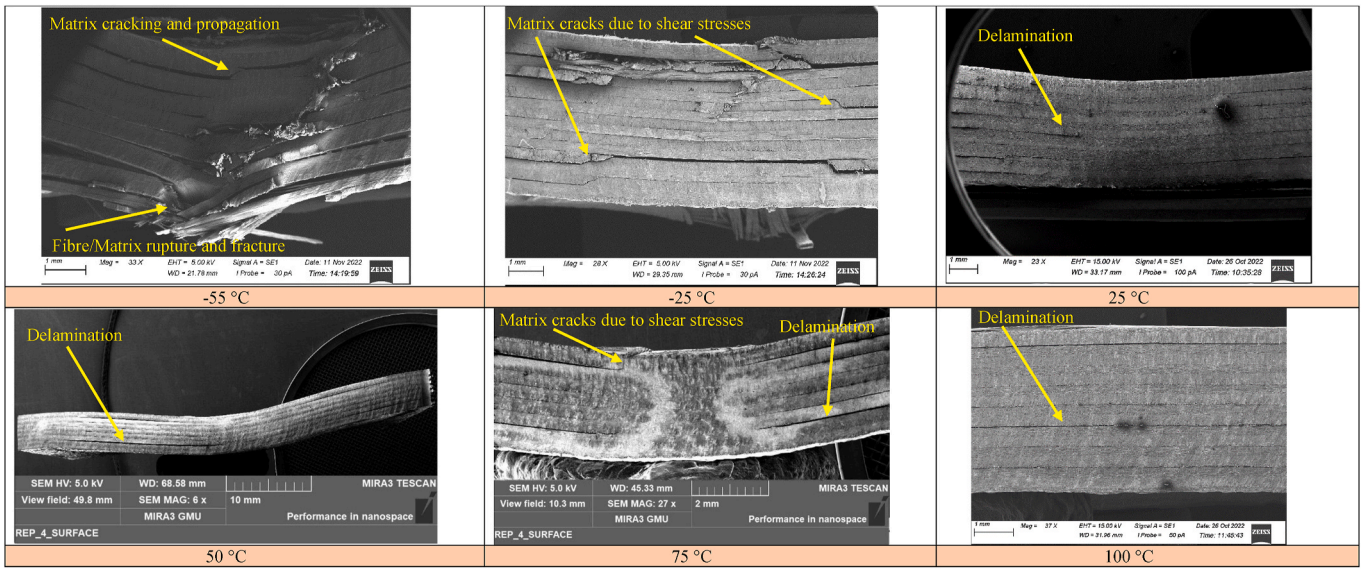

Fig. 8. SEM images for samples after impact at 150 J and different temperatures.

between (−25 to −55 °C) tests present similar behaviour to those for an impact energy of 150 J with the load increasing with time up to a maximum strength of about 28 kN as shown in Fig. 9a. The load then dropped sharply due mostly to fibre breakage in the fibre plies. While results for specimens tested at room temperature and high temperatures between (50–100 °C) exhibited higher compression strength approximately between (30–40 kN) demonstrating a higher resistance to impact when the glass transition temperature is reached reducing matrix cracking and matrix compression.

Specimens tested at room temperature exhibited similar behaviour to those tested at high temperatures. Similar behaviour was noticed for all specimens tested at high temperatures compared to those at low temperatures in terms of sharply decreasing compression strength directly after reaching ultimate strength with an additional failure mode – that of delamination in the interlaminar layers of the laminates. A sharp drop was also noticed for all tested specimens at the beginning of the test due to matrix cracking and initial matrix compression damage when the impactor first hits the specimen. Fig. 9b presents increasing out-of-plane displacements with increasing load until the ultimate compression strength is reached. At room temperature and cryogenic temperatures between (−25 to −55 °C), deformation reaches about (7 mm) at maximum compression strength due to fibre and matrix compression damage. Afterwards, the displacement decreases due to bridging of the fibres in the cross-ply laminates which causes high resistance to impact loads eventually reaching about half their maximum value at the end of the test. Again, similar to previous results of 150 J energy, as no penetration was occurred, thus impactor reflected back after hitting the specimen and this was noticed through reduction in the out-of-plane displacement which is reduced gradually up to the end of test. At high temperatures (50–100 °C) out-of-plane deformation reaches about (11–14 mm) at maximum compression strength due mostly to fibre and matrix compression damage. Similar to the behaviour at low temperatures, displacements show decreasing in their values as a result of fibre breakage, and also due to the delamination at the interlaminar layers which causes deformation in the negative out-of-plane axis direction opposite to the direction of the applied load until it reaches to approximately half its maximum value at the end of the test. Finally, as it can be seen from Fig. 9c, for all specimens tested, the kinetic energy reaches a maximum value of 225 J as planned then starts to reduce gradually for certain values then starts to recover at a time range (7–10 ms) onwards and remain constant up to the end of the test. Fig. 9 also shows the FE results which reveal an excellent correlation in terms of maximum impact strength for all specimens at different temperatures. At the high energy level 225 J, FE results show the predominant effect of the mechanical impact stresses over the thermal stresses causing specimens at cryogenic temperatures to fail at a lower strength of about 30 kN compared to those at room and high temperatures (25–75 °C) which failed at (35–40 kN). This is due to the high-velocity impact loads for the higher impact energy 225 J and the brittleness of the epoxy resin at low temperatures. At a high temperature of 100 °C impact strength was significantly reduced to about 30 kN due to the resin layers reaching their glass transition temperature. The second row of Fig. 9 also shows a good correlation with the displacements from the experiments. Finally, the observed energies are also perfectly predicted as the FE model considered the effect of both thermal and mechanical impact stresses simultaneously. As evident from SEM images (Fig. 10), the severity of the impact damage is increased, and fibre/matrix rupture can be clearly seen at cryogenic temperature which is similar to penetration damage that usually is seen in high-velocity impact scenarios. At higher temperatures, delamination is more common especially at the bottom layers of the specimens due to increased bending during impact. The through–thickness images (see Fig. 10) confirm that delamination and matrix cracks develop in the GFRP layers at higher temperatures (50–100 °C) and increase with the increment of applied impact energy. At cryogenic temperatures matrix cracks and partial fibre breakage are only seen at high energy levels and increase with the increment of applied impact energy. This damage mostly results from the penetration in the centre of the plates. The main reason for such penetration is that the resin layers become more brittle at cryogenic temperatures as discussed earlier.

4.4. Effect of temperature variation

4.4.1. Maximum impact force

Fig. 11 presents the maximum force and displacements for specimens under different impact energies 75, 150 and 225 J and temperatures from −55 to 100 °C. The experimental results show that at room temperature and cryogenic temperatures between −25 and −55 °C tests present similar behaviour under impact energy of 75 J with a maximum strength of about 25 kN. For higher temperatures between 50 and 100 °C there is a drop in ultimate strength which ranges between 22 and 14 kN. As discussed in section 4.1 this is probably due to resin layers reaching their glass transition temperature (T_g). The maximum force or ultimate strength for specimens tested under 150 J at cryogenic temperatures is

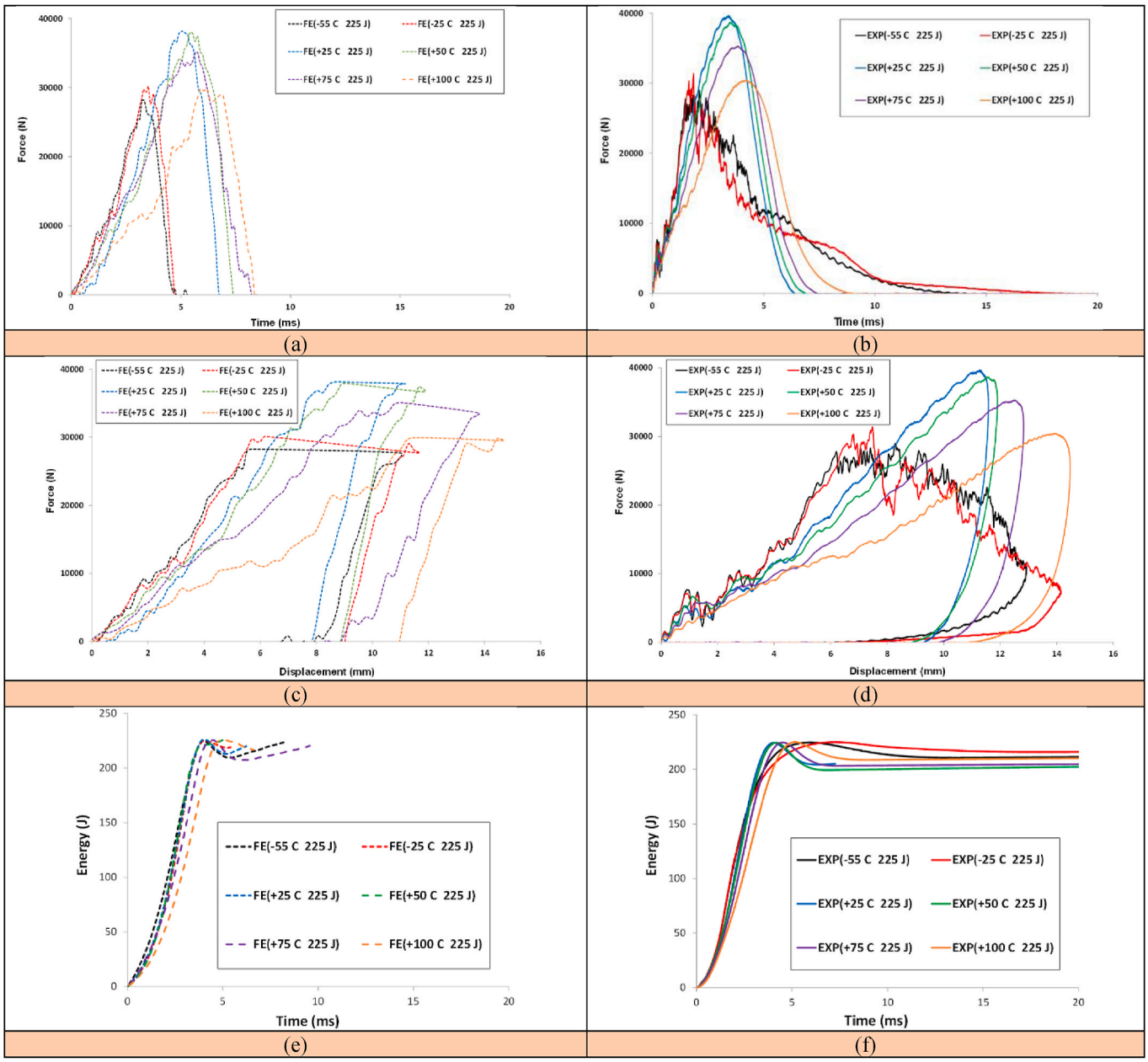

Fig. 9. Load vs. time; displacement curves and energy vs. time relation for S2/FM94 glass fibre plates under 225 J impact energy at a temperature range between −55, and 25, 25 [17], 50, 75 and 100 °C, FE and experimental results.

higher (33–35 kN) than those under 75 kJ and again drops at increased temperatures to between 31 and 22.5 kN for temperatures between 50 and 100 °C (again higher than at comparable temperatures under 75 kJ). For specimens tested under 225 J at cryogenic temperatures (−55 °C) the maximum strength is 32 kN similar to that for tests under an impact energy of 75 J. Results for room temperature and temperatures ranging between (25 and 50 °C) have a higher ultimate strength of 39 kN. It is thought that this is because at the higher velocity impacts at 225 J, the resin does not have enough time to reach to (T_g), resulting in it having higher strength. The FE results in Fig. 11 show an excellent correlation with the experimental ones in terms of maximum impact strength for all specimens across different temperatures and impact energy levels.

4.4.2. *Maximum impact displacement*

Maximum out-of-plane displacements for each of the different impact energies and temperatures are presented in Fig. 11. From the experimental results, under an impact energy of 75 J at room temperature and cryogenic temperatures between (−25 to −55 °C) tests present similar behaviour with a maximum displacement of about 6.5 mm. The results for higher temperatures between (50–100 °C) exhibited gradually increasing displacements ranging between (7–8.5 mm), due to resin layers reaching their glass transition temperature (T_g) as discussed in section 4.1. The displacement at cryogenic temperature is ~15–34 % less compared to those at higher temperature due to the decrease in the fracture strain at cryogenic temperatures leading to brittle fracture [49]. For an impact energy 150 J behaviour is similar to that for 75 J with tests at cryogenic temperatures having a maximum displacement of about 9 mm, and those at room temperature having a slightly higher displacement. The results for higher temperatures (50–100 °C) exhibited a gradually increasing maximum displacement (9.5–12 mm) slightly higher than for 75 J, due to the increasing temperature exacerbating the effects mentioned above. The results for impact energies of 225 J show slightly different behaviour from those for 75 J and 150 J. For temperatures between −25 and 50 °C the maximum displacement is

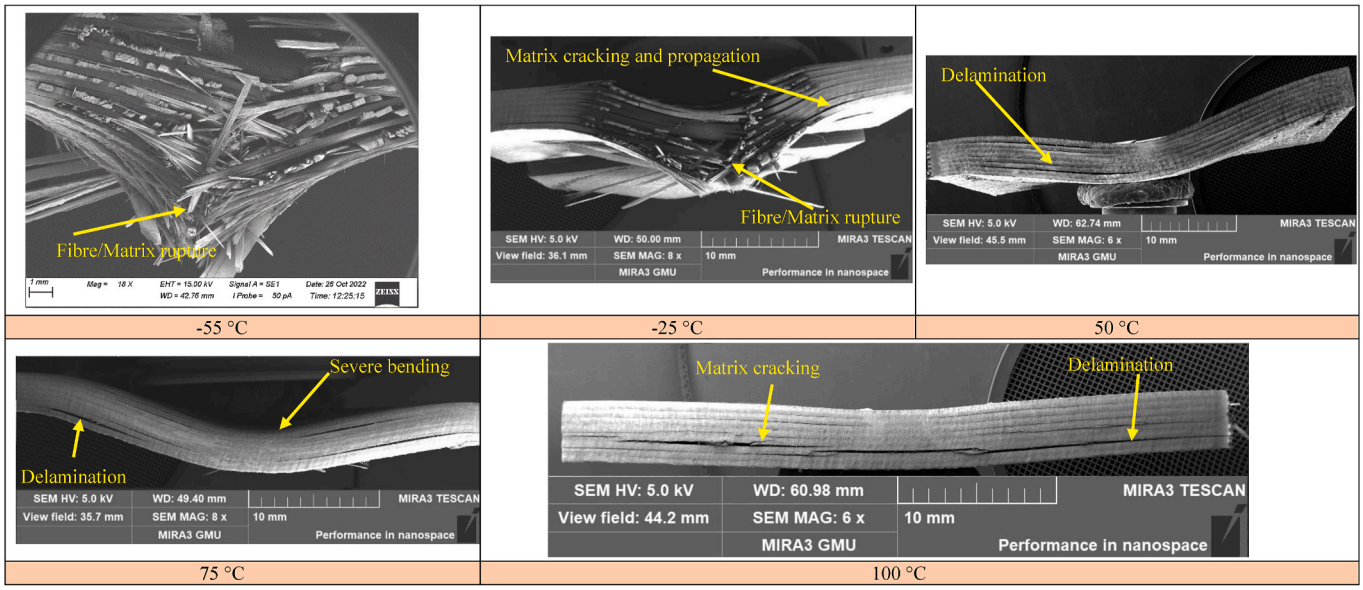

Fig. 10. SEM images for samples after impact at 225 J and different temperatures.

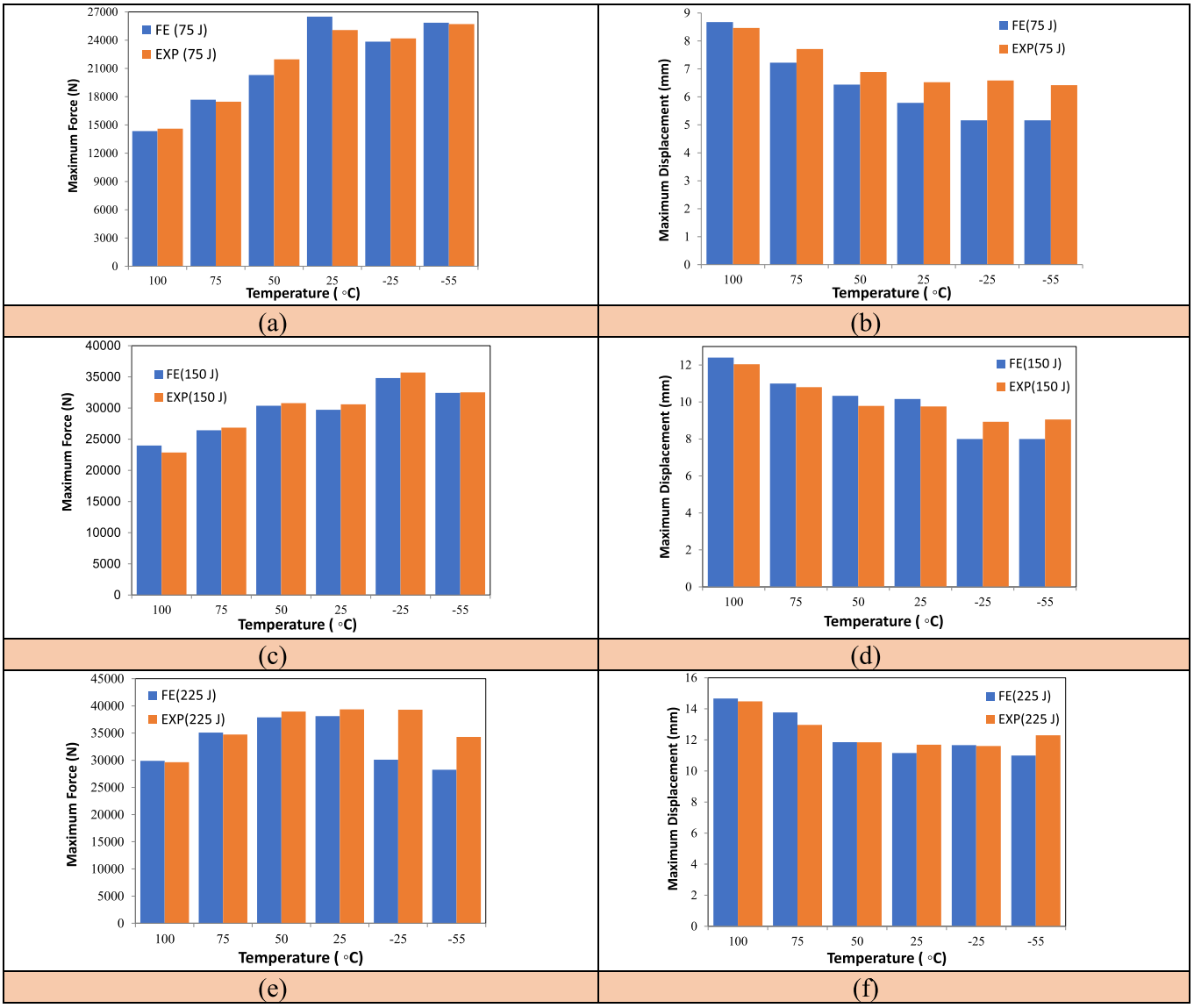

Fig. 11. Comparison of the level of maximum impact force and displacement at a temperature range between −55, and 25, 25 [17], 50, 75 and 100 °C under impact energies 75 J, 150 J and 225 J; FE and experimental results.

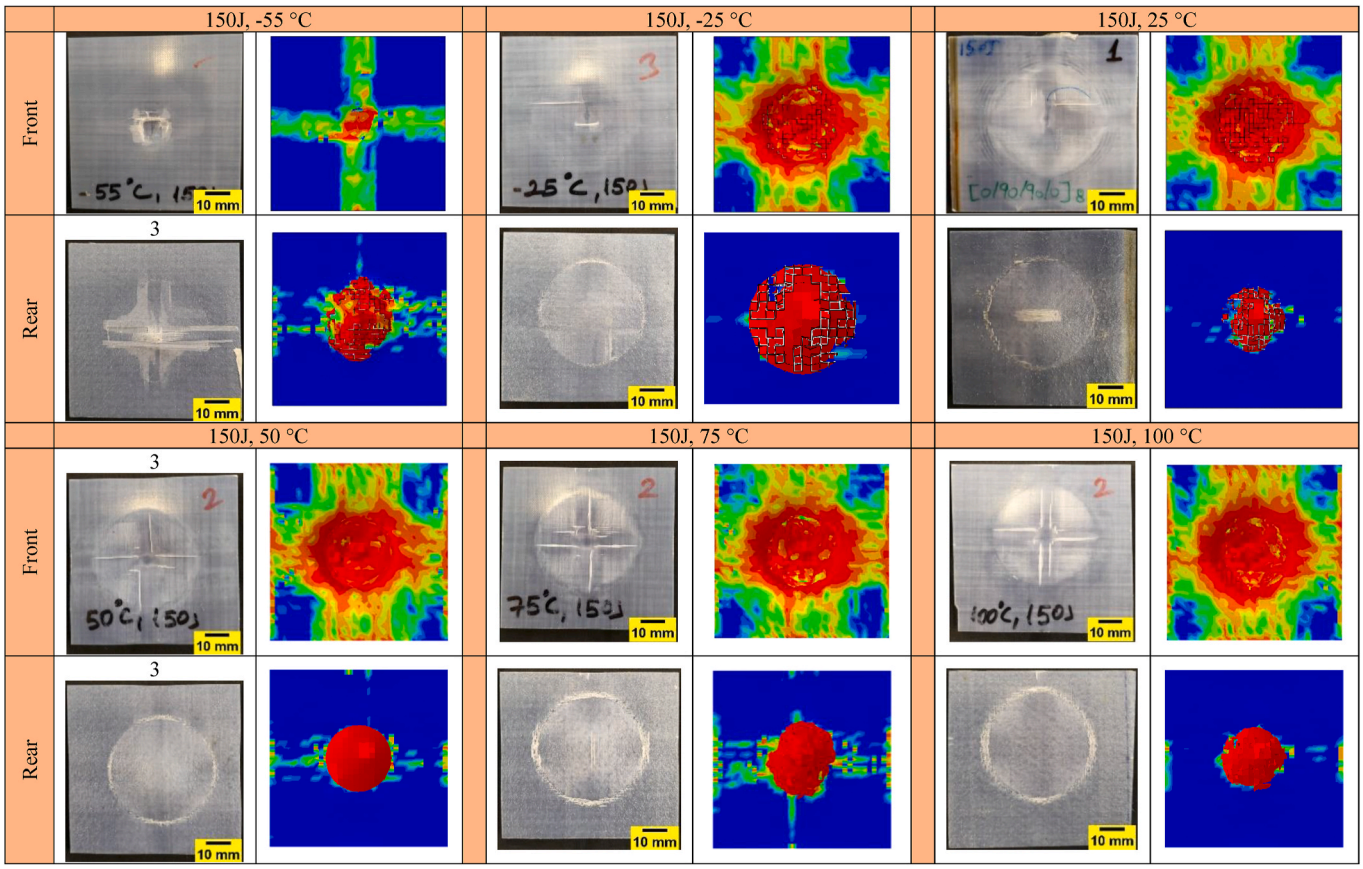

Fig. 12. Experimental and FE model results comparison for impact damage laminates (front and rear sides) after the impact at 150 J and for a temperature range between −55 and 100 °C.

approximately 12 mm, as a result of the high velocity of the impact load which means the resin does not have enough time to reach to T_g as discussed earlier. For higher temperatures between 75 and 100 °C there is a gradual increase in the maximum displacement between 13 and 14.5 mm, due to the increasing temperature being sufficient to enable the resin layers to reach the glass transition temperature (T_g) as mentioned earlier. Once again maximum impact displacement FE results present an excellent correlation with experiments.

4.5. Impact damage analysis

The effect of temperature variation on impact damage progression was also investigated both experimentally and numerically. Different behaviours in the form of different modes of failure were noticed for impact energies of 75, 150 and 225 J for temperatures ranging between −25 and 50 °C. FE results from Fig. 12 illustrating the predicted damage in the cohesive layers (SDEG) at 150 J also confirm that delamination and matrix cracks developed in the plies on the reverse side to the impact and increased with the increment of applied impact energy at room and higher temperatures. At cryogenic temperatures however, only matrix cracks and shear damage were noticed in the middle of the plates which also increased with the increment of applied impact energy. Results for other impact energies tested showed very similar behaviour.

The FE results in Fig. 13 represent the in-plane Mises stresses (S12) and confirm that delamination and matrix cracking develop near the front surface and increase with each increment of applied impact energy at room and high temperatures. Delamination is predicted by the orange segments (positive in-plane stress) in the first and third quarters of the impacted circular area, with blue segments in the second and fourth quarters of the impacted footprint circle (negative in-plane stress). At cryogenic temperatures, however, no delamination is predicted with only matrix cracking and shear damage. Again, these results are for 150 J, similar results are found for the other two impact energies.

The experimental impact damage shown previously is again supported by the damage predicted using the Hashin criterion as given in Fig. 14. FE results are for 150 J, and results for other impact energies showed similar behaviour. At higher temperatures a higher intensity of stresses is seen in the area surrounding the circular footprint of the impactor, this revealed the ability of the Hashin damage criterion to predict impact damage in composites. The micro-CT images shown previously in Fig. 4 confirm that matrix cracks damage occurred in this area, and this was confirmed via Hashin criterion FE analysis through matrix tension damage. Also, matrix compression damage from experiments seen in Fig. 3 was perfectly predicted by Hashin theory through the high activity of matrix compression variable in the middle front side of the specimens, while at room and cryogenic temperatures it predicted noticeable damage initiation and evolution within this area, a high out-of-plane deformation was noticed, mostly due to bending in the area surrounding the impactor head after impact which due to the high strength of the unidirectional fibre layers causes damage to be mostly limited to the resin layers. This was confirmed by the FE results which do not show any fibre tension or fibre compression damage using the Hashin criterion. Future analysis can be implemented to identify these damage mechanisms.

FE results from Fig. 15 represent through-thickness images for damage in cohesive layers (SDEG) and also confirm that delamination and matrix cracks develop in the GFRP layers at room and higher temperatures. Conversely, at cryogenic temperatures, no delamination in the interlaminar layers is noticed with only matrix cracks predicted in the middle of the plates, particularly at the impacted circular area. FE results are for impact energy at 150 J, and results for other impact

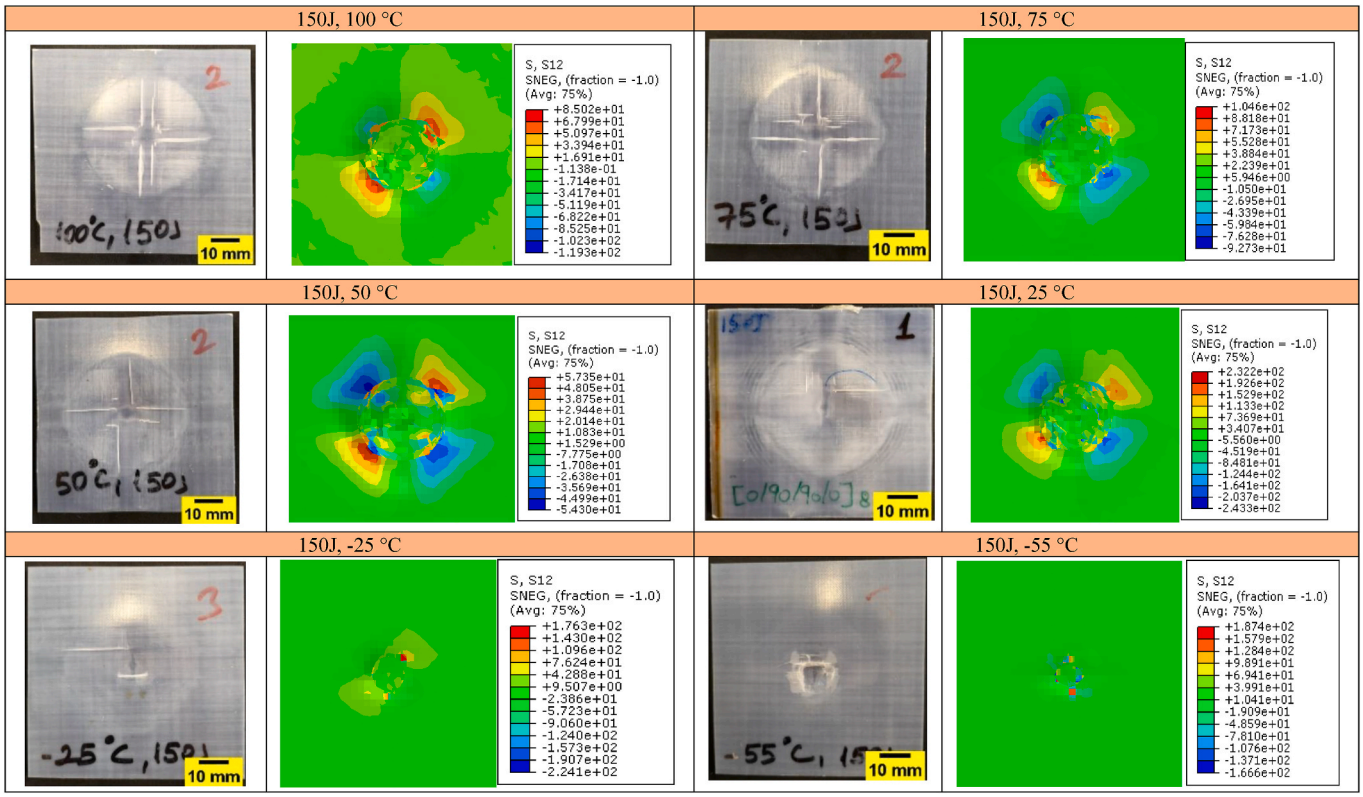

Fig. 13. Comparison between experimental results (front damage) and FE model results (Mises Stresses-in plane) after the impact at 150 J, for a temperature range between −55 and 100 °C.

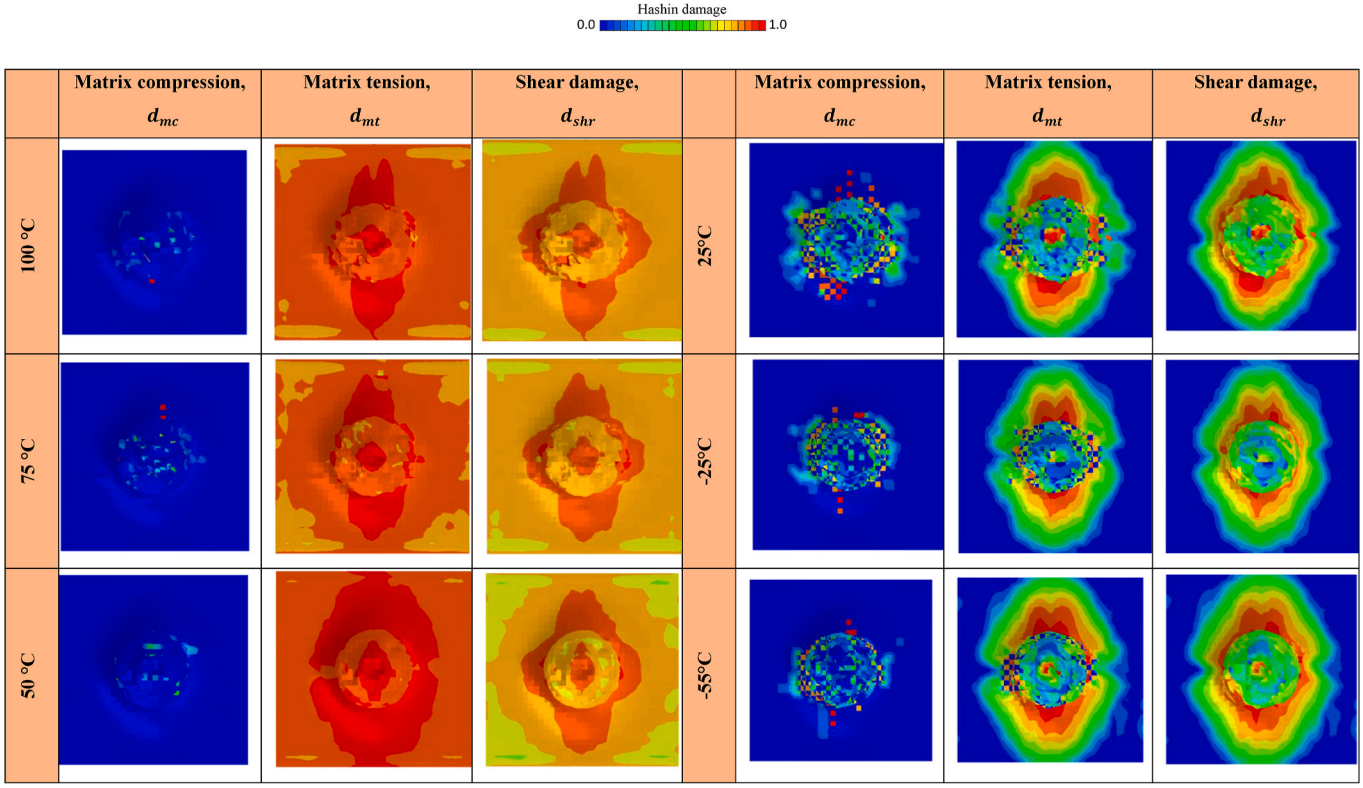

Fig. 14. FE results for damage evolution variables based on Hashin theory for the S2-glass fibre composite laminate, after the impact; impact at 150 J and for a temperature range between −55 and 100 °C.

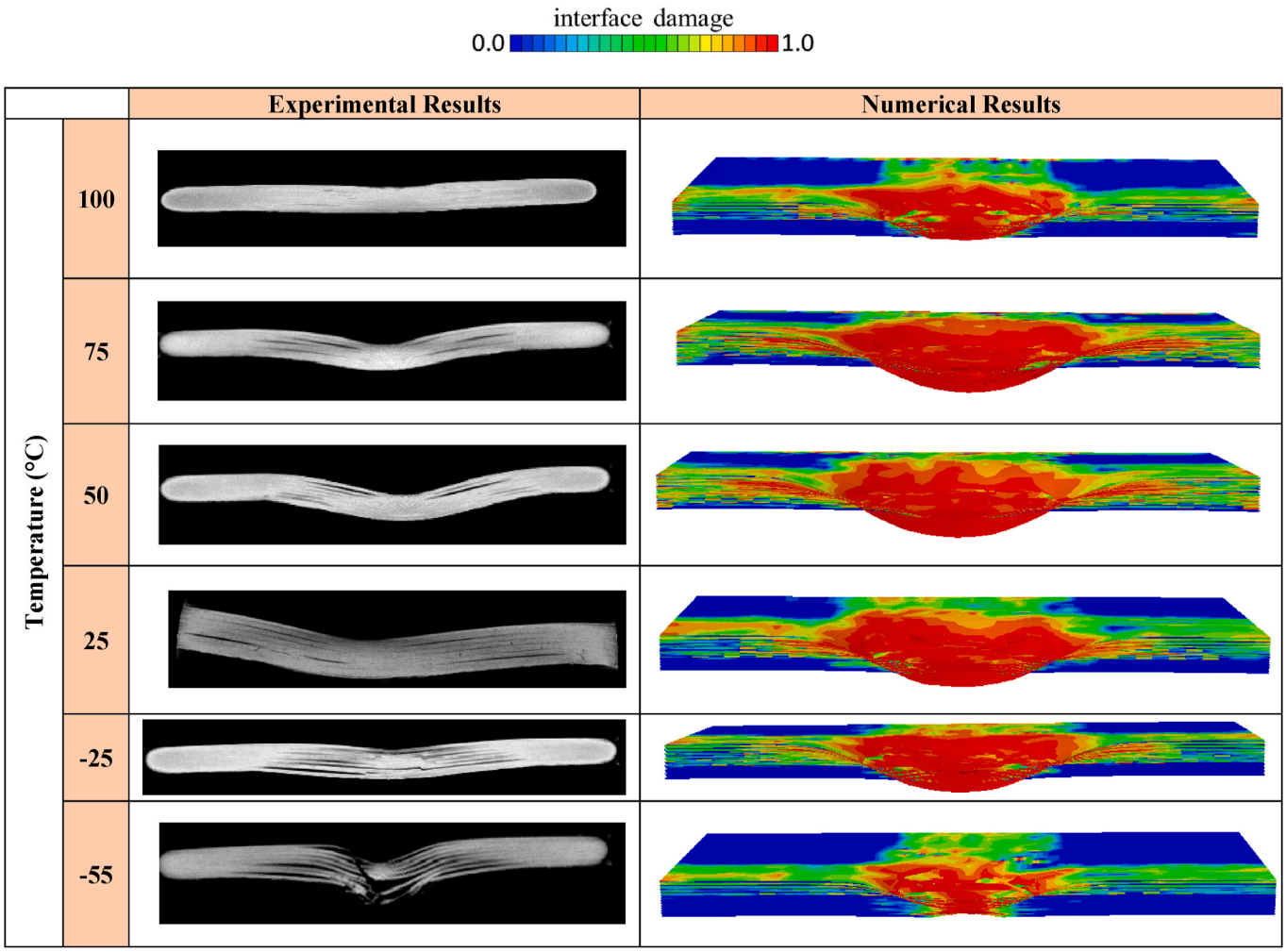

Fig. 15. Experimental through-thickness (C-scan images) and FE model (SDEG) results comparison for the damaged laminates after the impact at 150 J and for a temperature range between −55 and 100 °C.

energies exhibit similar behaviour. Bending represented by high curvature in the interlaminar layers for the impacted circular area was also successfully predicted using the cohesive zone model method available in Abaqus/Explicit analysis. The results confirm that the severity of damage increases with the energy level and reduction in temperature. At −25 °C (225 J), and −55 °C (125 and 225 J), the samples experienced partial penetration, some fibre/matrix petaling and fragmentation due to increased plastic deformation. Sever bending and bulge like dome can be clearly seen in samples impacted at 50 and 75 °C and at 150 and 225 J. This is mainly due to the increased elastic deformation of the samples at those temperatures which allowed the fibre/matrix to stretch further than at room or subzero temperatures.

5. Conclusions

The low-velocity impact behaviour of S2-glass fibre/FM94-epoxy composite laminates at three different impact energies and different temperatures ranges (including elevated and cryogenic temperatures) were investigated both experimentally and numerically. A total of fifty-four specimens were analysed, with an average of three specimens for each repeatability test. Impact damage characteristics of the specimens were investigated under cryogenic and high temperatures and results were evaluated based on the experiments and numerical analysis. The following conclusions are obtained.

(1) Temperature has a significant effect on the low-velocity impact response of laminated composites. More impact damage is induced in specimens impacted at lower temperatures than those at higher temperatures.
(2) Cross-ply composite laminates present higher impact strength at room and cryogenics temperatures compared with those at high temperatures.
(3) Delamination was observed in the impacted specimens at room and high temperatures, however, those tested under cryogenics temperatures did not show any delamination.
(4) Partial fibre breakage in the 0°, and 90° fibre plies was noticed in specimens tested at higher temperatures which aligned with the fibre orientation angles of cross-ply laminates.
(5) Matrix cracks (tension and compression) were more severe in the middle of GFRP specimens tested at cryogenic temperatures compared with those tested at high temperatures which led to penetration in the centre of the laminates at higher impact energy levels.
(6) Numerical results show excellent correlation with experimental results at all impact energy levels and for different temperature ranges.
(7) The Hashin damage criterion can accurately predict damage in composite laminates under low-velocity impact. The discrepancy between the experimental and numerical results was higher at lower impact energy of 75 J and cryogenic temperatures of −25 and −55 °C.

(8) Cohesive zone model theory is also able to predict damage in the interlaminar layers of composite laminates under low-velocity impact.

CRediT authorship contribution statement

Ahmad S.M. Al-Azzawi: Writing – review & editing, Writing – original draft, Software, Methodology, Formal analysis. **C.A. Featherston:** Writing – review & editing, Writing – original draft, Resources, Formal analysis. **Colin Lupton:** Writing – original draft, Software, Formal analysis. **Chulin Jiang:** Writing – review & editing, Writing – original draft, Validation, Software, Formal analysis. **Antigoni Barouni:** Writing – review & editing, Writing – original draft, Validation, Software, Formal analysis. **Ugur Koklu:** Writing – original draft, Resources, Methodology, Investigation, Formal analysis, Conceptualization. **Khaled Giasin:** Writing – review & editing, Writing – original draft, Visualization, Validation, Resources, Project administration, Methodology, Investigation, Formal analysis, Conceptualization.

Declaration of competing interest

The authors declare that they have no known competing financial interests or personal relationships that could have appeared to influence the work reported in this paper.

Data availability

Data will be made available on request.

Acknowledgements

The authors would like to thank Mr Garry Shipley at Cardiff School of Engineering for their kind assistance with the manufacturing of the specimens.

Appendix A. Supplementary data

Supplementary data to this article can be found online at https://doi.org/10.1016/j.compositesb.2024.111786.

Appendices

Appendix A: Table showing summary of past studies on low velocity impact of glass fibre composites.

Material	Stacking sequence	Thickness (mm)	Temperature (°C)	Energy (J)	FE	Notes	Ref
E-glass/ epoxy	[0°/90°/+45°/ −45°]	3	20, −20, −60	10, 30, 50, 70	No	Perforation ↑ as temperature ↓	[24]
E-glass/ epoxy	[0] and [0°/90°]	3.2	−20,0,10,20	12.8	No	Cross-ply laminates have better impact resistance	[16]
E-glass/ epoxy	[0°/30°/60°/90°]	2.9	Room temperature	10, 20, 30, 40	Yes	Impact velocity and energy affect damage differently	[50]
S2-glass/ epoxy	[0/90/+ 45/− 45] [0/90/90/0] [+45/− 45] [0]	4.25	Room temperature	75, 150, 225	Yes	[0/90/90/0] showed superior resistance to impact among other configurations	[17]
E-glass/ epoxy	Woven	~2.5	−50, 25, 70, 120	8, 15, 25	No	Ductility index ↑ as temperature ↑	[28]
GFRP	Woven	1.46	−173, −74, 22	NA	No	Size and depth of damage ↓ as temperature ↓	[25]
E-glass/ epoxy	Filament winding	2.375	−196, 0, 22, 50, 100	5, 7.5, 10	No	Stiffness ↑ and deflection ↓ as temperature ↓	[51]
E-glass/ epoxy	[0°/90°] woven	5, 7, 10	−25, 20, 100	50, 100, 150	No	Max displacement ↓ with ↑ of laminate thickness and as temperature ↓	[52]
E-glass/ epoxy	[0°/90°] woven	2.1, 3.5, 5	−50, −25, room temperature	41–111	No	Absorbed energy is affected by thickness and temperature differently	[53]

References

[1] Airbus. *TCDS No.: EASA.A.004 AIRBUS A330*.[26/02/2024]; Available from:: https://www.easa.europa.eu/en/downloads/7518/en.
[2] National Research Council. D.o.E.a.L.S., board on environmental studies and toxicology, committee on air quality in passenger cabins of commercial aircraft. The airliner cabin environment and the health of passengers and crew 2002;344. National Academies Press.
[3] Accelerated aging of materials and structures: the effects of long-term elevated-temperature exposure. Washington, DC: The National Academies Press; 1996. 65 DOI: doi:10.17226/9251.Available from: https://nap.nationalacademies.org/catalog/9251/accelerated-aging-of-materials-and-structures-the-effects-of-long.
[4] Ostré B, Bouvet C, Minot C, Aboissière J. Experimental analysis of CFRP laminates subjected to compression after edge impact. Compos Struct 2016;152:767–78. https://doi.org/10.1016/j.compstruct.2016.05.068.
[5] Wisnom MR, Hallett SR. The role of delamination in strength, failure mechanism and hole size effect in open hole tensile tests on quasi-isotropic laminates. Compos Appl Sci Manuf 2009;40(4):335–42. https://doi.org/10.1016/j.compositesa.2008.12.013.
[6] Shi Y. T.S., C. Soutis, Modelling damage evolution in composite laminates subjected to low velocity impact. Compos Struct 2012;94(9):2902–13. https://doi.org/10.1016/j.compstruct.2012.03.039.
[7] Hall YLJ, Brooks ZEC, Liu RA, Kinloch H, Dear, J.P AJ. Damage and energy absorption behaviour of composite laminates under impact loading using different impactor geometries. Compos Struct 2023. https://doi.org/10.1016/j.compstruct.2023.117259.
[8] Shah SZH, Karuppanan S, Megat-Yusoff PSM, Sajid Z. Impact resistance and damage tolerance of fiber reinforced composites: a review. Compos Struct 2019;217:100–21. https://doi.org/10.1016/j.compstruct.2019.03.021.
[9] Barile C, Casavola C, Pappalettera G, Kannan VP. Application of different acoustic emission descriptors in damage assessment of fiber reinforced plastics: a comprehensive review. Eng Fract Mech 2020;235:107083. https://doi.org/10.1016/j.engfracmech.2020.107083.
[10] Liu X, Cheng L, Zhang L, Dong N, Wu S, Meng Z. Tensile properties and damage evolution in a 3D C/SiC composite at cryogenic temperatures. Mater Sci Eng 2011;528(25):7524–8. https://doi.org/10.1016/j.msea.2011.06.050.

[11] Yang FJ, Cantwell WJ. Impact damage initiation in composite materials. Composites Science and Technology. 70(2): pp. 336–342, https://doi.org/10.1016/j.compscitech.2009.11.004; 2010.

[12] Dokos L, Mowlem M, Chambers A, Brambilla G, Pruneri V. Low velocity impact detection and damage assessment in composite materials using fibre Bragg grating sensors. Proc. ICCM 2001.

[13] Cook P, Alavija A, Wildy S. Identification and characterisation of delamination damage in composites utilising embedded optical strain gauges. 9th Australasian Congress on Applied Mechanics 2017. Engineers Australia.

[14] Zhang ZY, Richardson MOW. Visualisation of barely visible impact damage in polymer matrix composites using an optical deformation and strain measurement system (ODSMS). Compos Appl Sci Manuf 2005;36(8):1073–8. https://doi.org/10.1016/j.compositesa.2004.10.035.

[15] Shyr T-W, Pan Y-H. Impact resistance and damage characteristics of composite laminates. Compos Struct 2003;62(2):193–203. https://doi.org/10.1016/S0263-8223(03)00114-4.

[16] Ibekwe SI, Mensah PF, Li G, Pang S-S, Stubblefield MA. Impact and post impact response of laminated beams at low temperatures. Compos Struct 2007;79(1):12–7. https://doi.org/10.1016/j.compstruct.2005.11.025.

[17] Giasin K, Dhakal HN, Featheroson CA, Pimenov DY, Lupton C, Jiang C, Barouni A, Koklu U. Effect of fibre orientation on impact damage resistance of S2/FM94 glass fibre composites for aerospace applications: an experimental evaluation and numerical validation. Polymers 2022;14(1):95. https://doi.org/10.3390/polym14010095.

[18] García-Moreno I, Caminero MÁ, Rodríguez GP, López-Cela JJ. Effect of thermal ageing on the impact damage resistance and tolerance of carbon-fibre-reinforced epoxy laminates. Polymers 2019;11(1):160. https://doi.org/10.3390/polym11010160.

[19] Vieille B, Albouy W, Bouscarrat D, Taleb L. High-temperature fatigue behaviour of notched quasi-isotropic thermoplastic and thermoset laminates: influence of matrix ductility on damage mechanisms and stress distribution. Compos Struct 2016;153:311–20. https://doi.org/10.1016/j.compstruct.2016.06.015.

[20] Papa I, Donadio F, Sánchez Gálvez V, Lopresto V. On the low- and high-velocity impact behaviour of hybrid composite materials at room and extreme temperature. J Compos Mater 2022;56(1):31–42. https://doi.org/10.1177/00219983211047688.

[21] Gieleta R, Kruszka L. Dynamic testing of reinforced glass fibre–epoxy composite at elevated temperatures. Strength Mater 2002;34(3):238–41. https://doi.org/10.1023/A:1016254213429.

[22] López-Puente J, Zaera R, Navarro C. The effect of low temperatures on the intermediate and high velocity impact response of CFRPs. Compos B Eng 2002;33(8):559–66. https://doi.org/10.1016/S1359-8368(02)00065-3.

[23] Gómez-del Río T, Zaera R, Barbero E, Navarro C. Damage in CFRPs due to low velocity impact at low temperature. Compos B Eng 2005;36(1):41–50. https://doi.org/10.1016/j.compositesb.2004.04.003.

[24] Icten BM, Atas C, Aktas M, Karakuzu R. Low temperature effect on impact response of quasi-isotropic glass/epoxy laminated plates. Compos Struct 2009;91(3):318–23. https://doi.org/10.1016/j.compstruct.2009.05.010.

[25] Ma H-l, Jia Z, Lau K-t, Leng J, Hui D. Impact properties of glass fiber/epoxy composites at cryogenic environment. Compos B Eng 2016;92:210–7. https://doi.org/10.1016/j.compositesb.2016.02.013.

[26] Shahabaz SM, Sharma S, Shetty N, Shetty SD. G.M. M.C, influence of temperature on mechanical properties and machining of fibre reinforced polymer composites: a review. Engineered Science 2021;16:26–46. https://doi.org/10.30919/es8d553.

[27] Salehi-Khojin A, Mahinfalah M, Bashirzadeh R, Freeman B. Temperature effects on Kevlar/hybrid and carbon fiber composite sandwiches under impact loading. Compos Struct 2007;78(2):197–206. https://doi.org/10.1016/j.compstruct.2005.09.005.

[28] Salehi-Khojin A, Bashirzadeh R, Mahinfalah M, Nakhaei-Jazar R. The role of temperature on impact properties of Kevlar/fiberglass composite laminates. Compos B Eng 2006;37(7):593–602. https://doi.org/10.1016/j.compositesb.2006.03.009.

[29] R. Gieleta, L.K., dynamic testing of reinforced glass fibre–epoxy composite at elevated temperatures. Strength Mater 2002;(3):34. https://doi.org/10.1023/A:1016254213429.

[30] Ilaria Papa FD, Sánchez Gálvez Vicente, Lopresto Valentina. On the low- and high-velocity impact behaviour of hybrid composite materials at room and extreme temperature. J Compos Mater 2022;56(1):31–42. https://doi.org/10.1177/00219983211047688.

[31] Yan Li FW, Huang Chenguang, Ren Jianting, Wang Donghong, Kong Jie, Liu Tao, Long Laohu. Impact damage reduction of woven composites subject to pulse current. Nat Commun 2023:14. https://doi.org/10.1038/s41467-023-40752-6.

[32] Vlot A, Gunnink JW. Springer DOI. Fibre metal laminates: an introduction 2001. https://doi.org/10.1007/978-94-010-0995-9.

[33] Giasin K, Barouni A, Dhakal HN, Featherson C, Redouane Z, Morkavuk S, Koklu U. Microstructural investigation and hole quality evaluation in S2/FM94 glass-fibre composites under dry and cryogenic conditions. Journal of Reinforced Plastics 2020. https://doi.org/10.1177/0731684420958479.

[34] Hongkarnjanakul N, Bouvet C, Rivallant S. Validation of low velocity impact modelling on different stacking sequences of CFRP laminates and influence of fibre failure. Compos Struct 2013;106:549–59. https://doi.org/10.1016/j.compstruct.2013.07.008.

[35] Sun XC, Kawashita LF, Kaddour AS, Hiley MJ, Hallett SR. Comparison of low velocity impact modelling techniques for thermoplastic and thermoset polymer composites. Compos Struct 2018;203:659–71. https://doi.org/10.1016/j.compstruct.2018.07.054.

[36] Heimbs S, Heller S, Middendorf P, Hähnel F, Weiße J. Low velocity impact on CFRP plates with compressive preload: test and modelling. Int J Impact Eng 2009;36(10):1182–93. https://doi.org/10.1016/j.ijimpeng.2009.04.006.

[37] Falcó O, Lopes CS, Sommer DE, Thomson D, Ávila RL, Tijs BHAH. Experimental analysis and simulation of low-velocity impact damage of composite laminates. Compos Struct 2022;287:115278. https://doi.org/10.1016/j.compstruct.2022.115278.

[38] Sugiman S, Crocombe AD. The static and fatigue response of metal laminate and hybrid fibre-metal laminate doublers joints under tension loading. Compos Struct 2012;94:2937–51. https://doi.org/10.1016/j.compstruct.2012.03.013.

[39] Seyed-Yaghoubi A, Liaw B. Experimental and numerical approaches on behavior of Glare 5 beams: influences of thickness and stacking sequence. In: Allemang R, Niezrecki C, Blough J, editors. Proceedings of the 30th IMAC, J. D. C. New York: Springer; 2012. p. 7–16. https://doi.org/10.1007/978-1-4614-2419-2_2 (Eds.), Ed., ed.

[40] Alderliesten R. Fatigue crack propagation and delamination growth in glare. Delft University of Technology; 2005.

[41] Rathnasabapathy M, Mouritz A, Orifici A. Numerical investigation of fibre-metal laminates subject to impact damage. in Proceedings of 18th International Conference on Composite Materials. 18th International Conference on Composite Materials 2011.

[42] Hashin Z. Failure criteria for unidirectional fibre composites. ASME Journal of Applied Mechanics 1980;47(2):329–34. https://doi.org/10.1115/1.3153664.

[43] Dassault Systemes. Abaqus analysis user's manual 2019.

[44] Kawashita LF, Hallett SR. A crack tip tracking algorithm for cohesive interface element analysis of fatigue delamination propagation in composite materials. Int J Solid Struct 2012;49:2898–913. https://doi.org/10.1016/j.ijsolstr.2012.03.034.

[45] Daiyan H, Andreassen E, Grytten F, Lyngstad OV, Luksepp T, Osnes H. Low-velocity impact response of injection-moulded polypropylene plates – Part 1: effects of plate thickness, impact velocity and temperature. Polym Test 2010;29(6):648–57. https://doi.org/10.1016/j.polymertesting.2010.05.003.

[46] Sápi Zsombor, B R. Properties of cryogenic and low temperature composite materials – a review. Cryogenics 2020:111. https://doi.org/10.1016/j.cryogenics.2020.103190.

[47] Teixeira de Freitas S, Sinke J. Failure analysis of adhesively-bonded metal-skin-to-composite-stiffener: effect of temperature and cyclic loading. Compos Struct 2017;166:27–37. https://doi.org/10.1016/j.compstruct.2017.01.027.

[48] Khan R. Fiber bridging in composite laminates: a literature review. Compos Struct 2019;229:111418. https://doi.org/10.1016/j.compstruct.2019.111418.

[49] Li Y, Meng J, Luo J, Wang P, Ma J, Zhao Z, Lei H. Cryogenic mechanics and damage behaviors of carbon fiber reinforced polymer composites. Compos Appl Sci Manuf 2023;169:107484. https://doi.org/10.1016/j.compositesa.2023.107484.

[50] Karakuzu R, Erbil E, Aktas M. Impact characterization of glass/epoxy composite plates: an experimental and numerical study. Compos B Eng 2010;41(5):388–95. https://doi.org/10.1016/j.compositesb.2010.02.003.

[51] Kara M, Arat M, Uyaner M. Low velocity impact response and damages of GFRP composite tubes under room and cryogenic temperatures. J Compos Mater 2021;55(24):3567–77. https://doi.org/10.1177/00219983211029368.

[52] Weng J, Wen W, Zhang H. Study on low-velocity impact and residual strength at high temperatures of composite laminates. Proc Inst Mech Eng G J Aerosp Eng 2019;233(3):1106–23. https://doi.org/10.1177/09544100177481.

[53] Russo P, Langella A, Papa I, Simeoli G, Lopresto V. Thermoplastic polyurethane/glass fabric composite laminates: Low velocity impact behavior under extreme temperature conditions. Compos Struct 2017;166:146–52. https://doi.org/10.1016/j.compstruct.2017.01.054.